Complement C3-Targeted Gene Therapy Restricts Onset and Progression of Neurodegeneration in Chronic Mouse Glaucoma

Alejandra Bosco,[1] Sarah R. Anderson,[1,4] Kevin T. Breen,[1,4,5] Cesar O. Romero,[1] Michael R. Steele,[1] Vince A. Chiodo,[2] Sanford L. Boye,[2] William W. Hauswirth,[2] Stephen Tomlinson,[3] and Monica L. Vetter[1]

[1]Department of Neurobiology and Anatomy, School of Medicine, University of Utah, Salt Lake City, UT, USA; [2]Department of Ophthalmology, University of Florida, Gainesville, FL, USA; [3]Department of Microbiology and Immunology, Medical University of South Carolina, Charleston, SC, USA

Dysregulation of the complement system is implicated in neurodegeneration, including human and animal glaucoma. Optic nerve and retinal damage in glaucoma is preceded by local complement upregulation and activation, but whether targeting this early innate immune response could have therapeutic benefit remains undefined. Because complement signals through three pathways that intersect at complement C3 activation, here we targeted this step to restore complement balance in the glaucomatous retina and to determine its contribution to degeneration onset and/or progression. To achieve this, we combined adeno-associated virus retinal gene therapy with the targeted C3 inhibitor CR2-Crry. We show that intravitreal injection of AAV2.CR2-Crry produced sustained Crry overexpression in the retina and reduced deposition of the activation product complement C3d on retinal ganglion cells and the inner retina of DBA/2J mice. This resulted in neuroprotection of retinal ganglion cell axons and somata despite continued intraocular pressure elevation, suggesting a direct restriction of neurodegeneration onset and progression and significant delay to terminal disease stages. Our study uncovers a damaging effect of complement C3 or downstream complement activation in glaucoma, and it establishes AAV2.CR2-Crry as a viable therapeutic strategy to target pathogenic C3-mediated complement activation in the glaucomatous retina.

INTRODUCTION

Glaucoma irreversibly impairs vision by progressive neurodegeneration of retinal ganglion cells (RGCs). Axonopathy precedes neuronal loss, with the earliest damage detectable in unmyelinated axons at the optic nerve head (ONH), followed by gradual axonal and neuronal decline and dropout with advancing age.[1] The pathobiology of this neurodegenerative disease remains unclear due to manifold processes and risk factors, including age, ethnic group, and elevated intraocular pressure (IOP).[2] Current therapies can successfully lower IOP and decelerate, but not halt, the progression of neurodegeneration.[3] Thus, developing neuroprotective approaches to interrupt progression is a primary goal.[4] To be effective, therapies should target pathways and processes that have been demonstrated to drive neurodegeneration in animal models and human glaucoma.

Emerging research ties glaucomatous neurodegeneration to complement dysregulation in the retina and ONH, identifying C1q and C3 as candidate therapeutic targets.[5,6] Complement is an innate immune molecular network that acts to remove pathogens, damaged cells, and immune complexes.[7] C3 is the central complement component and point of convergence for three main initiation pathways (classical, alternative, and lectin).[8] C1q is the pattern recognition molecule that canonically initiates the classical pathway, but it has broader functions beyond the complement system.[9] In the CNS, C1q and C3 tag synapses, as well as damaged and apoptotic neurons, for clearance by microglia or infiltrating macrophages.[10] Neurons, astrocytes, microglia, and peripheral monocytes are local sources of complement proteins, especially during damage or disease.[11] Thus, in addition to traditional roles in serum immunosurveillance, complement is now recognized for its central roles in CNS development and adult homeostasis, as well as in pathology, including aging and neurodegeneration.[12,13] How local CNS complement contributes protective, reparative, or pathogenic roles is under active study.

In the retina, changes in complement expression underlie aging and a number of pathologies, including glaucoma.[14] Retinal proteome and transcriptome analyses have detected C1q and C3 upregulation in human glaucoma[15–17] and ocular hypertension,[18,19] as well as across animal models of induced IOP elevation.[5,15,19–27] Expression of C1q mRNA was detected in RGCs and ONH microglia and/or macrophages.[25,27,28] These findings place local complement dysregulation during early stages of glaucoma, preceding optic nerve (ON) degeneration.

The DBA/2J mouse strain develops progressive RGC degeneration with variable age of onset, exhibiting disease features relevant to

human glaucoma.[29] Systemic knockout of C1q and C3 genes in the DBA/2J was the first attempt to assess the impact of complement activation in glaucoma. C1q deficiency was neuroprotective, delaying, but not halting, the progression of ON degeneration.[27,28,30] Unpredictably, C3 deficiency worsened degeneration before the terminal stage.[26] Both IOP elevation and anterior segment disease were delayed by C1q, but not C3, deficiency. Of note, DBA/2J mice are deficient for C5 and terminal pathway activation, implying that upstream complement components are sufficient to drive neurodegeneration, although restoring C5 worsens its severity.[31] These divergent outcomes of C1q and C3 deficiency suggest that there may be activation of multiple complement pathways during the course of chronic glaucoma, each functioning with partial independence, possibly at different stages and contributing pathogenic or protective roles. Since gene knockout cannot distinguish systemic from local effects, developmental from adult effects, or onset versus progression of neurodegeneration, the therapeutic potential of modulating complement activation in the glaucomatous retina remains undefined.

Inhibitors affecting the central step of formation of C3 convertase formation and cleavage and activation have become a focus for the development of therapeutics that effectively modulate complement activation, regardless of the initiation pathway.[32] Furthermore, the deposition of C3 activation fragments iC3b, C3dg, and C3d, covalently bound to cell surfaces, serves as a long-lived indicator of local complement activation amenable to imaging in the living animal or *ex vivo* and as a ligand for CR2-fused inhibitors to achieve localized regulation of complement activation.[8,33,34] In rodents, the main regulator of C3 convertase formation is Crry, a structural and functional ortholog of human complement receptor 1 (CR1).[35,36] Endogenous Crry is expressed on brain microglia and astrocytes,[37] as well as across the retina and retinal pigment epithelium (RPE),[38] and it is upregulated in the DBA/2J retina and ONH.[27] Site-targeted CR2-Crry, which directs soluble Crry to activated C3 deposits,[39] inhibits local complement activation 10-fold more actively than untargeted soluble Crry.[33]

Endogenous complement inhibitors have long been used in C3-targeted strategies to interrupt initiating complement pathways and broadly balance complement activation.[32] To overcome adverse systemic effects and effectively inhibit local C3 activation, targeted approaches have been designed to selectively supply complement regulators to sites of cleaved C3 deposition on cells and tissues.[33] CR2-Crry is a fusion protein of the murine C3 convertase inhibitor Crry (complement receptor 1-related protein Y) and the C3d/dg complement receptor 2 (CR2) moiety, which targets Crry to sites of activated C3 deposition.[39] CR2-Crry has been proven neuroprotective in the ischemic brain,[39–41] as well as in the experimental autoimmune encephalomyelitis model of multiple sclerosis.[42] Systemically administered CR2-Crry crosses defective blood-brain barriers in these models of acute CNS injury,[34,43] but it would have limited capacity to cross an intact barrier.

Ocular gene therapy viral vectors, such as adeno-associated virus (AAV), have been used to provide the diseased retina with local and permanent expression of Crry and other inhibitors, to chronically attenuate complement activation in models of age-related macular degeneration.[44–46] Serotype 2 AAV vectors yield widespread transduction of the inner retina and RGCs 1 month after intravitreal injection in the mouse eye[47] and over 10 months in the DBA/2J retina.[48–51] Thus, stable expression of targeted complement inhibitors via AAV gene therapy should be a viable approach to chronically attenuate complement activation during DBA/2J glaucoma progression.

Here we used targeted gene therapy to test whether C3 activation contributes to the onset and/or late progression of neurodegeneration in glaucoma by using AAV2 to deliver CR2-Crry. DBA/2J mice received intravitreal injections of AAV2.CR2-Crry at 7 months of age, when most ONs are structurally intact, and they were aged and evaluated for alterations in timing and severity of neurodegeneration relative to AAV2.GFP and naive controls. We provide evidence that AAV2.CR2-Crry retinal gene therapy effectively increases Crry expression and dampens C3d deposition in RGCs, which results in significant long-term neuroprotection of ONs and retina. Degeneration was almost eliminated at 10 months, and progression to terminal stage was suppressed at 12 and 15 months. Thus, AAV2.CR2-Crry ocular gene therapy provides a precise and translatable strategy to locally balance retinal C3 activation during disease progression and reduce neurodegeneration in chronic glaucoma.

RESULTS

Intravitreal AAV2.CR2-Crry Limits the Deposition of C3d on RGCs

To allow local expression of targeted inhibitors of C3 activation to the retina of DBA/2J mice, we adopted ocular gene therapy using high-efficiency triple Y-F mutant capsid AAV2 vectors, which result in widespread and stable transduction of RGCs and inner retina in adult mice.[47] We performed bilateral, intravitreal injections of AAV2.GFP reporter at 10^{10} total vector genomes per eye in 7-month-old DBA/2J mice, and we confirmed efficient transduction of the inner retina in 10-month-old mice, consistent with previous reports of DBA/2J viral gene therapy.[48–51] Retinal whole mounts and radial sections showed GFP expression in the nerve fiber layer (NFL) and ganglion cell layer (GCL) (Figures 1A and 1B). GFP expression was also observed in interneurons and Müller glia (Figure 1B), but it was not detectable in photoreceptors, microglia, vasculature, or the RPE. Coimmunostaining with the RGC-specific transcription factor Brn3a and use of Thy1[+/CFP] DBA/2J reporter mice[52] confirmed AAV2.GFP expression in RGCs and their axons across all quadrants and eccentricities (data not shown). The ON showed GFP expression along axons within the proximal segment (Figure 1C). This spread of AAV2.GFP transduction in the DBA/2J retina and ON is consistent with previous reports of AAV2-GFP transduction, which also showed its presence in the lateral geniculate nucleus and superior colliculus.[53] AAV2.GFP expression in the retina was first detected 2–3 weeks post-injection and peaked by 1 month, with expression persisting for at least 5 months (data not shown).
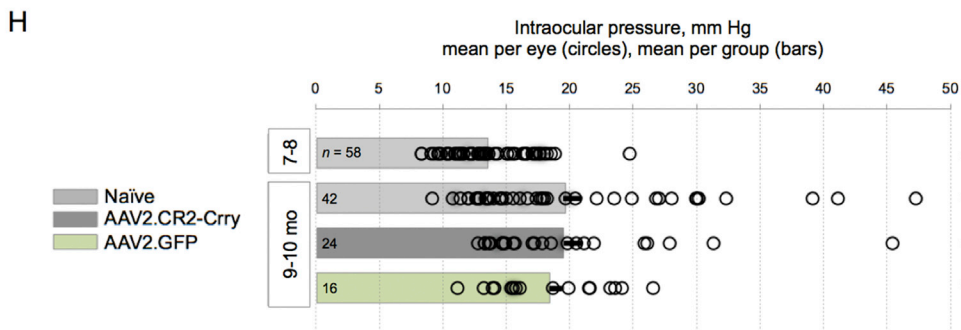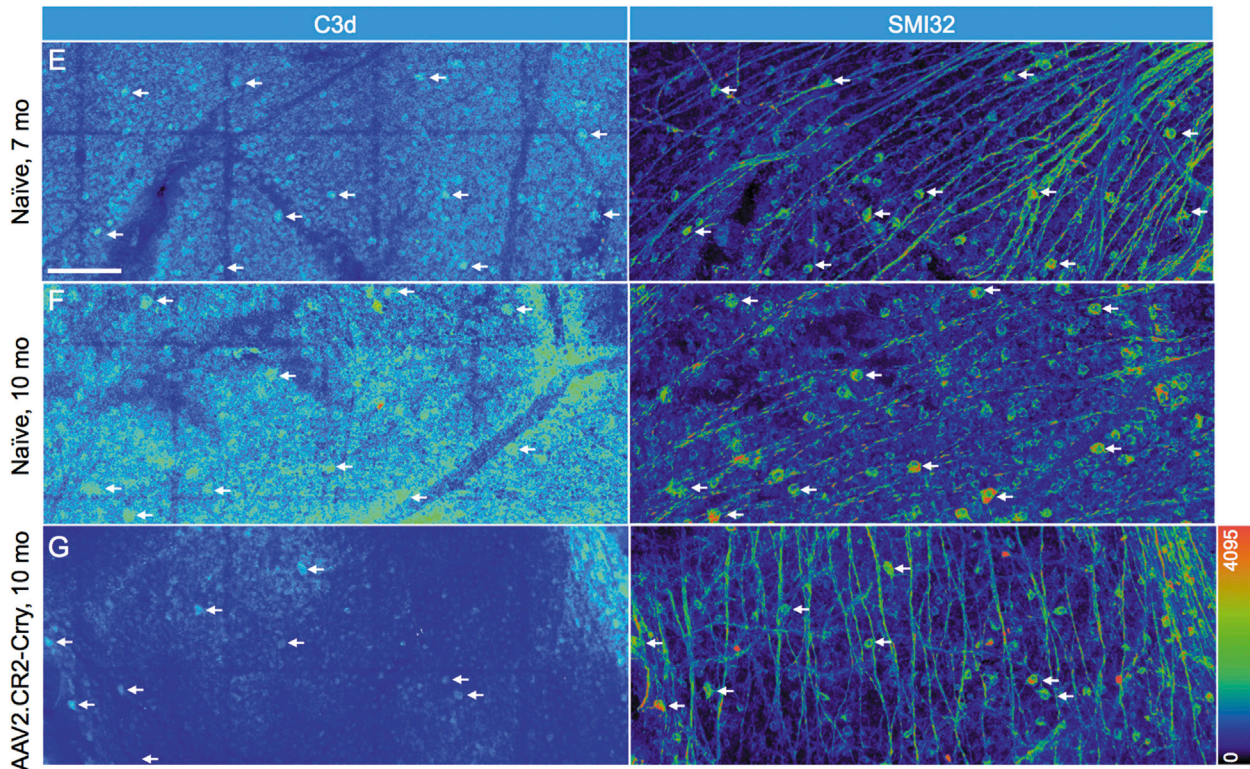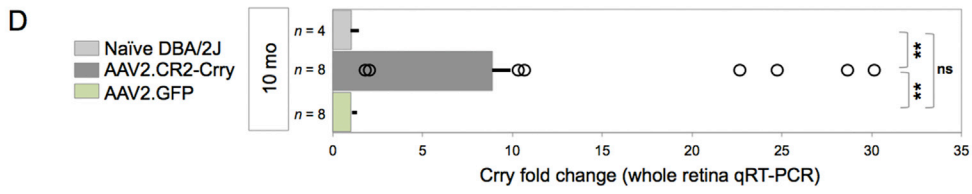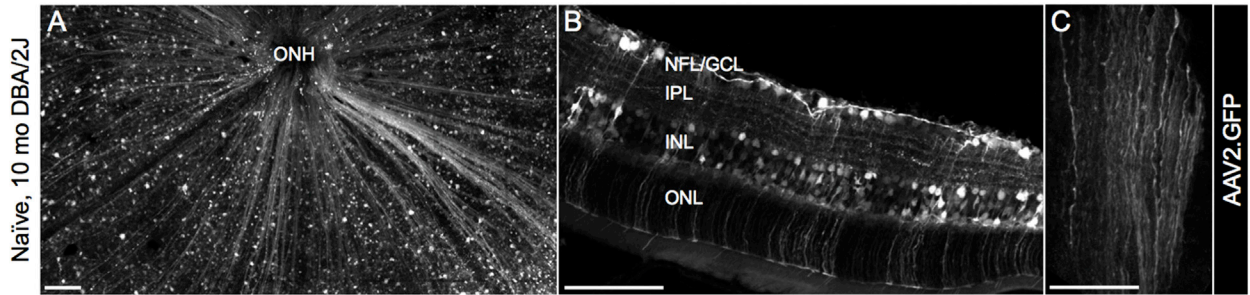
(legend on next page)

To selectively reduce complement activation in the glaucomatous retina, the original construct for recombinant CR2-Crry fusion cDNA[39] was packaged in YF mutant capsid AAV2 vector;[47,54] then 7-month-old DBA/2J mice received single injections of AAV2.CR2-Crry bilaterally, and they were aged to 10 months together with naive littermates. To detect overexpression of Crry, whole-retina qPCR was performed to measure the relative fold change of total Crry (endogenous plus exogenous) and to compare treated and naive retinas. Expression of Crry mRNA showed an 8-fold mean increase in AAV2.CR2-Crry-treated retinas (n = 8) over naive (n = 4) and AAV2-GFP (n = 8), with 10- to 30-fold upregulation in 6 of 8 treated retinas (Figure 1D). One-way ANOVA revealed a significant difference among the three groups (p < 0.001). Levels of Crry in AAV2.CR2-Crry were significantly elevated from naive and from AAV2.GFP controls by a Tukey's multiple comparisons test (p < 0.01 and p = 0.0011, respectively), whereas AAV2.GFP controls were not significantly different from the naive condition (Table 1). Due to differences in variances between samples, we confirmed these results with an unpaired Student's t test with Welch's correction.

To gauge C3 activation in the retina, we performed immunostaining of retinal whole mounts to detect the C3 breakdown product C3d, which is deposited on cell surfaces.[33,55] Confocal microscopy of naive 7-month-old DBA/2J mice showed C3d staining of cell somata in the GCL, with variable levels of fluorescence intensity across large retinal sectors (Figure 1E). This deposition was also detectable by immunostaining in retinas at 5 months of age (data not shown). To confirm labeling of RGCs, we performed coimmunostaining of αRGCs with the SMI32 neurofilament antibody,[50,56,57] which consistently revealed C3d deposition in αRGCs across multiple eyes (n = 8; Figure 1E). C3d deposition persisted in 10-month-old naive DBA/2J mice, which showed labeling of the GCL throughout the entire retina, with generally higher intensity levels relative to 7-month-old naive mice (Figure 1F). Use of Thy1[+/CFP] DBA/2J reporter mice and triple immunostaining showed C3d colocalization to Thy1-expressing RGCs, which colabeled with SMI32 and/or gamma-synuclein in retinal whole mounts (Figure S1A). The C3d antibody has been used in previous studies;[58–60] to further test its specificity, we immunostained retinas from non-glaucoma Gpnmb[WT] DBA/2J mice prepared as

radial sections, and we observed negligible C3d staining, comparable to negative immunostaining controls of naive DBA/2J retinas omitting primary antibody (data not shown).

Retinas treated with AAV2.CR2-Crry at 7 months exhibited a general reduction in C3d deposition at 10 months relative to naive retinas at the same age, with retinal whole mounts displaying uniformly low levels of C3d expression throughout the GCL and fewer cells with high C3d deposition (Figure 1G). Dystrophic SMI32-labeled αRGCs were stained for C3d, while most αRGCs with healthy morphology had dim or undetectable C3d staining. We did not observe C3d deposition on microglia of naive or treated retinas (Figure S1B), unlike reports of C3d localization to brain microglia in patients with multiple sclerosis and other neurodegenerative conditions.[61–63] We did detect C3d on GFAP+ parenchymal astrocytes in some naive retinas aged 10 months (data not shown). Together, these observations suggest that AAV2.CR2-Crry is able to decrease the activation of C3 throughout the retina in DBA/2J mice aged 7–10 months.

AAV2.CR2-Crry Retinal Gene Therapy Does Not Alter the Typical Elevation of IOP in DBA/2J

To determine whether the IOP of mice treated with AAV2.CR2-Crry would elevate with similar time course and values as naive DBA/2J mice, we compared IOPs from 7 to 10 months of age. By a Kruskal-Wallis test, we found a significant difference across all groups (p < 0.0001). As expected, IOP increased significantly in naive mice from 7–8 months (13.52 mm Hg ± 0.42 SEM, n = 58) to 9–10 months (19.6 ± 1.37 mm Hg, n = 42; p < 0.01 by Kolmogorov-Smirnov) (Figure 1H), consistent with published results.[64,65] Importantly, we found a comparable and significant IOP elevation from 7–8 to 9–10 months for both AAV2.CR2-Crry-treated (19.48 ± 1.53 mm Hg, n = 24) and AAV2.GFP-injected eyes (18.40 ± 1.15 mm Hg, n = 16; p < 0.01 each; Table 2). Furthermore, there was not a statistical difference in the mean IOP among 9- to 10-month-old naive, AAV2.CR2-Crry, and AAV2.GFP conditions by Kruskal-Wallis comparison (p = 0.812). These results were confirmed with a post hoc Dunn's multiple comparisons test (Table 2). These findings indicate that intravitreal gene therapy with AAV2.CR2-Crry or AAV2.GFP did not reduce or delay IOP elevation in treated DBA/2J eyes.

Figure 1. C3d Deposition on RGCs and GCL Is Lessened by Retinal Crry Overexpression

(A) Representative retinal whole mount of 10-month-old DBA/2J mice injected with AAV2-GFP at 7 months, showing widespread GFP localization to RGCs and their axons. Confocal image of the NFL and GCL shows the innermost 25 μm below the vitreal surface, seen as maximum-intensity projection and low magnification. (B) Radial section across the retina, displaying GFP expression in RGC somata and axons, inner plexiform layer (IPL) interneurons, and Müller glia. Confocal image shows a 10-μm maximum-intensity projection. (C) ON showing GFP content in axons along a longitudinal cryosection, viewed in a single slice (0.8 μm thick), ~2 mm behind the retina. (D) Mean fold change of Crry mRNA expression in whole retinas from 10-month-old mice treated with AAV2.CR2-Crry or AAV2.GFP relative to age-matched naive retinas measured by qRT-PCR. Error bars represent mean ± SEM. Dots represent fold change in single retinas. **p < 0.01 each (see Table 1). (E–G) Confocal images of retinal whole mounts spanning the NFL and GCL (~40-μm maximum-intensity projections; mid-periphery), showing single channels in pseudocolors to emphasize variations in signal intensity. (E) Naive retina, representative of 7-month-old DBA/2J, double-immunostained for C3d and SMI32. C3d localized to GCL cells throughout large sectors (left) and to SMI32+ αRGCs (arrows). (F) Naive retina, representative of 10-month-old mice, which displays intense C3d deposits throughout the GCL and in SMI32+ αRGCs (arrows). (G) AAV2.CR2-Crry-treated retina, representative of 10-month-old mice, showing C3d immunostaining in the GCL confined to reduced retinal sectors and to a few declining SMI32+ αRGCs (arrows). Scale bars, 100 μm (A and B) and 50 μm (C–F). (H) Bar graph of IOP (mean ± SEM per group) showing that, at 9–10 months of age, eyes in all groups underwent a significant increase compared to 7- to 8-month naive eyes (p < 0.01). The IOP of individual eyes (circles) exhibit extensive overlap at 9–10 months, regardless of condition, with means not significantly different between naive and AAV2.CR2-Crry or AAV2.GFP (see Table 2). Number of eyes per group is indicated within each bar. Significance level is indicated as follows: ns, not significant; *p < 0.05; **p < 0.01; and *** (p < 0.001), for this and the following figures.

Table 1. Crry mRNA Expression

	One-Way ANOVA		Tukey's Multiple Comparisons Test	F-Test to Compare Variances	Unpaired t Test
10-month-old naive		versus GFP	p = 0.9978[b]	p = 0.3071	p = 0.7833
	p = 0.0006[a,b]	versus Crry	p = 0.0052[a,b]	p = 0.0195[a]	*p = 0.0041[a]
10-month-old CR2-Crry		versus GFP	p = 0.0011[a,b]	p < 0.0001[a]	*p = 0.0047[a]
10-month-old GFP		–	–	–	–

Statistical comparisons for Delta CT values (Figure 1D). *Welch's correction.
[a]Significant differences.
[b]The values reported in the Results.

Complement Inhibition Reduces RGC Degeneration Rates and Severity

To establish whether the local attenuation of retinal C3 activation could alter the course and severity of RGC somal degeneration and loss, we performed intravitreal injection of AAV2.CR2-Crry in 7-month-old DBA/2J female mice and aged them to 10 months. We then examined their level of RGC preservation *ex vivo*, relative to both age- and gender-matched control AAV2.GFP-treated and naive eyes. To detect RGCs with persistent transcriptional integrity, retinal whole mounts were immunostained with a Brn3 antibody that recognizes all three isoforms of Brn3 transcription factors,[66–68] since their downregulation serves as an early marker of RGC dysfunction.[66–69] Confocal microscopy images spanning the GCL of entire whole mounts showed a range in the density of Brn3+ RGCs. All experimental groups showed healthy retinas with uniformly dense Brn3+ RGC mosaics (Figures 2A and 2D) and declining retinas with Brn3+ RGC loss across sectors radiating from the ONH across one or more quadrants (Figures 2B and 2E). However, degenerative retinas with prevalent low Brn3+ RGC densities and sectorial depletion were common in naive (Figure 2C) and AAV2.GFP control eyes, but they were infrequent in AAV2.CR2-Crry eyes.

To represent the variable patterns and severity of RGC loss that are characteristic in DBA/2J glaucoma progression,[57] in individual retinas we estimated RGC preservation by counting Brn3+ nuclei within the densest sector at the mid-periphery of each quadrant, and also we estimated RGC depletion by measuring the extent of retinal sectors with $\leq$500 Brn3+ nuclei/mm^2 (Figure 2F). Analysis of mean Brn3+ cell densities revealed a large variability in all experimental conditions at 10 months of age, ranging from 0 to almost 3,000 cells/mm^2 (Figure 2G). We found a significant difference across all 10-month groups by Kruskal-Wallis (p < 0.01). Due to the variability of the model and, therefore, non-normal distribution of preserved Brn3+ cell density, we performed pairwise comparisons of these distributions by nonparametric Kolmogorov-Smirnov tests (Table 3). There were significant differences between 10-month-old AAV2.CR2-Crry-treated retinas (n = 36) compared to both naive (p = 0.01; n = 29) and AAV2.GFP retinas (p < 0.05; n = 28), but there was no significant difference between naive and AAV2.GFP retinas (p = 0.103). The nonparametric Mann-Whitney U test, which is more sensitive to differences in medians, confirmed the significant difference of AAV2.CR2-Crry compared to naive (p < 0.001), but it found no

significant difference compared to the AAV2.GFP group (p = 0.117; Table 3), suggesting a partial effect from AAV2-GFP delivery over naive retinas.

To better represent the stages of retinal degeneration per condition, we compared the proportions of retinas at each level of Brn3+ RGC preservation (highest mean density) as pre-degenerative (3,000–2,000 RGCs/mm^2), declining (2,000–1,000 RGCs/mm^2), or degenerative (1,000–0 RGCs/mm^2). At 10 months, AAV2.CR2-Crry-treated retinas had 31%, 61%, and 8% pre-degenerative, declining, and degenerative Brn3+ RGC densities, respectively; whereas naive retinas had 4%, 48%, and 48%; and AAV2.GFP-treated retinas had 25%, 32%, and 43% pre-degenerative, declining, and degenerative densities, correspondingly (Figure 2H). Application of a chi-square (χ^2) test for association indicated significant differences between AAV2.CR2-Crry and both naive (p < 0.001) and AAV2.GFP (p < 0.01), but not in AAV2.GFP versus naive retinas (p = 0.057; Table 4).

Next, to determine the magnitude of RGC depletion, we measured the extent of sectorial depletion (in degrees) of Brn3+ RGCs (less than 500 nuclei/mm^2), and we report the proportion of retinas with either no (0-degree), partial (1- to 359-degree), or complete (360-degree) depletion (Figure 2I). At 10 months, the AAV2.CR2-Crry group (n = 34) had 73% of retinas with no depletion, 23% with partial, and 4% with complete depletion versus 32%, 32%, and 36% in naive eyes (n = 25) and 42%, 31%, and 27% in AAV2.GFP controls (n = 26). A chi-square (χ^2) test for association revealed significant differences of AAV2.CR2-Crry from either naive (p < 0.001) or AAV2.GFP (p < 0.01) conditions, whereas AAV2.GFP was not significantly different from naive retinas (p = 0.522; Table 5). There was a significant difference across all 10-month-old groups of mean degrees of Brn3+ RGC depletion (p = 0.0011, Kruskal-Wallis). Furthermore, there was a significant difference at 10 months for AAV2.CR2-Crry retinas (39 ± 15 degrees) compared to either naive (160 ± 32 degrees, p < 0.02) or AAV2.GFP (154 ± 31 degrees, p < 0.02) (Figure 2J), and there was no significant difference between naive and AAV2-GFP control groups by Kolmogorov-Smirnov tests (p = 0.999; Table 6). This denotes a robust absence of low-density sectors in AAV2.CR2-Crry-treated retinas, indicating reduced progression toward terminal degeneration stages relative to both naive and

Table 2. Intraocular Pressure

	Normality (Shapiro-Wilk)	Kruskal-Wallis	Kruskal-Wallis		Dunn's Multiple Comparisons	Kolmogorov-Smirnov	Mann-Whitney U
7- to 8-month-old naive	p = 0.015[a]		–	versus 9-10 naive	p = 0.0002[a]	p = 0.0053[a,b]	p < 0.0001[a]
				versus 9-10 Crry	p = 0.0001[a]	p < 0.0005[a,b]	p < 0.0001[a]
				versus 9-10 GFP	p = 0.0019[a]	p = 0.0042[a,b]	p = 0.0001[a]
9- to 10-month-old naive	p = 0.000[a]	p < 0.0001[a]		versus GFP	p > 0.9999	p = 0.5273	p = 0.7208
				versus CR2-Crry	p > 0.9999	p = 0.5976	p = 0.5228
9- to 10-month-old CR2-Crry	p = 0.000[a]		p = 0.8119[b]	versus GFP	p > 0.9999	p = 0.9868	p = 0.9077
9- to 10-month-old GFP	p = 0.434			–	–	–	–

Statistical comparisons for mean IOP per group (Figure 1H).
[a]Significant differences.
[b]The values reported in the Results.

AAV2-GFP-treated retinas. Overall, these findings show that, by multiple measures, AAV2.CR2-Crry results in potent preservation of Brn3+ RGCs at 10 months.

Since disruption of complement pathways has been reported to have variable effects on disease progression,[26,28] we also performed analysis at 12 months focusing on naive retinas, which show a well-characterized progression of RGC degeneration,[57,70] compared to AAV2.CR2-Crry-treated retinas. The distributions of Brn3+ cell density showed progressive loss in both groups (Figure 2K). However, AAV2.CR2-Crry-treated retinas (n = 18) retained significantly higher RGC densities compared to naive retinas (p < 0.01 by Kolmogorov-Smirnov and p < 0.001 by Mann-Whitney U test; n = 19; Table 3). When we assessed RGC preservation at 12 months of age, we found that AAV2.CR2-Crry retinas were 11%, 50%, and 39% pre-degenerative, declining, and degenerative, respectively, in stark contrast to naive retinas that were either declining or degenerative (19% and 81%, respectively) (Figure 2L). A chi-square (χ^2) test for association indicated a significant difference between AAV2.CR2-Crry and naive retinas (p < 0.01; Table 4). Furthermore, analysis of RGC depletion at 12 months of age found that 53% AAV2.CR2-Crry retinas had no depletion, 41% had partial, and 6% had complete depletion, in contrast to 6%, 19%, and 75%, respectively, in untreated naive retinas (Figure 2M). AAV2.CR2-Crry was significantly different from naive (p < 0.001, chi-square (χ^2) test for association; Table 5). At 12 months of age, the mean depleted angle had increased in AAV2.CR2-Crry (108 ± 32 degrees) (Figure 2N), but it was still significantly different from the untreated group (297 ± 31 degrees; p < 0.001 by Kolmogorov-Smirnov; Table 6). The combined analysis of Brn3+ RGC maintenance and depletion demonstrates that AAV2.CR2-Crry treatment resulted in the preservation of higher densities of Brn3+ RGC that were uniform across quadrants in the majority of retinas. Thus, AAV2.CR2-Crry treatment results in a strong reduction in the progression toward Brn3+ RGC loss.

The neuroprotective effect of AAV2.CR2-Crry on RGC somal density may be more robust than estimated by Brn3 immunostaining, given

the downregulation of this transcription factor in DBA/2J retinas at the ages analyzed.[66,67] In line with this, AAV2.CR2-Crry treatment of a subset of 7-month-old Thy1[+/CFP] DBA/2J reporter mice[52] resulted in 10-month-old healthy retinas with uniformly dense mosaics of RGCs co-expressing Brn3 and Thy1 (Figure 2O), but also in retinas with homogeneous high densities of Thy1-expressing RGCs but loss of Brn3 expression (Figure 2P). Mean Thy1-positive GCL nuclear counts showed 2,031 ± 64 in AAV2.CR2-Crry versus 731 ± 157 nuclei/mm^2 in naive (n = 8 and 15, respectively), which is relatively higher than the mean density of Brn3-positive RGCs (1,565 ± 106 nuclei/mm^2) in AAV2.CR2-Crry retinas. This suggests transcriptional changes in persistent RGCs and a potential underestimate of RGC somal survival by AAV2.CR2-Crry therapy if analysis is based only on Brn3 expression.

Intraretinal Axons Preserve Their Fasciculation Integrity after CR2-Crry Treatment

To define whether the neuroprotective effect of CR2-Crry on RGC somata extended to the unmyelinated axon, we evaluated the integrity of axon fasciculation in the NFL. Intraretinal RGC axons were visualized by confocal microscopy images of whole-mount retinas immunostained for phosphorylated neurofilament (pNF), a cytoskeletal marker extensively used to selectively track both healthy and degenerative RGC axons.[57,66,67,71] Naive, healthy retinas displayed axons uniformly segregated in tightly packed fascicles across all quadrants in 10-month-old DBA/2J mice (Figure 3A, A'), whereas degenerative retinas exhibited defasciculation, with fascicle thinning and solitary axons (Figure 3B, B').

The mean density of pNF+ RGC axons per fascicle for individual retinas was estimated by counting the number of axons per bundle across 250 μm at the healthiest sector of each retinal quadrant (Figure 3C; see the Materials and Methods for details). As a baseline, we measured 3.6 ± 0.18 axons/fascicle (mean ± SEM, n = 5 retinas; data not shown) in non-glaucoma retinas from Gpnmb[WT] DBA/2J mice at 10 months of age (Figure S2). At 10 months, there was a significant difference across groups (p = 0.0083, one-way ANOVA;
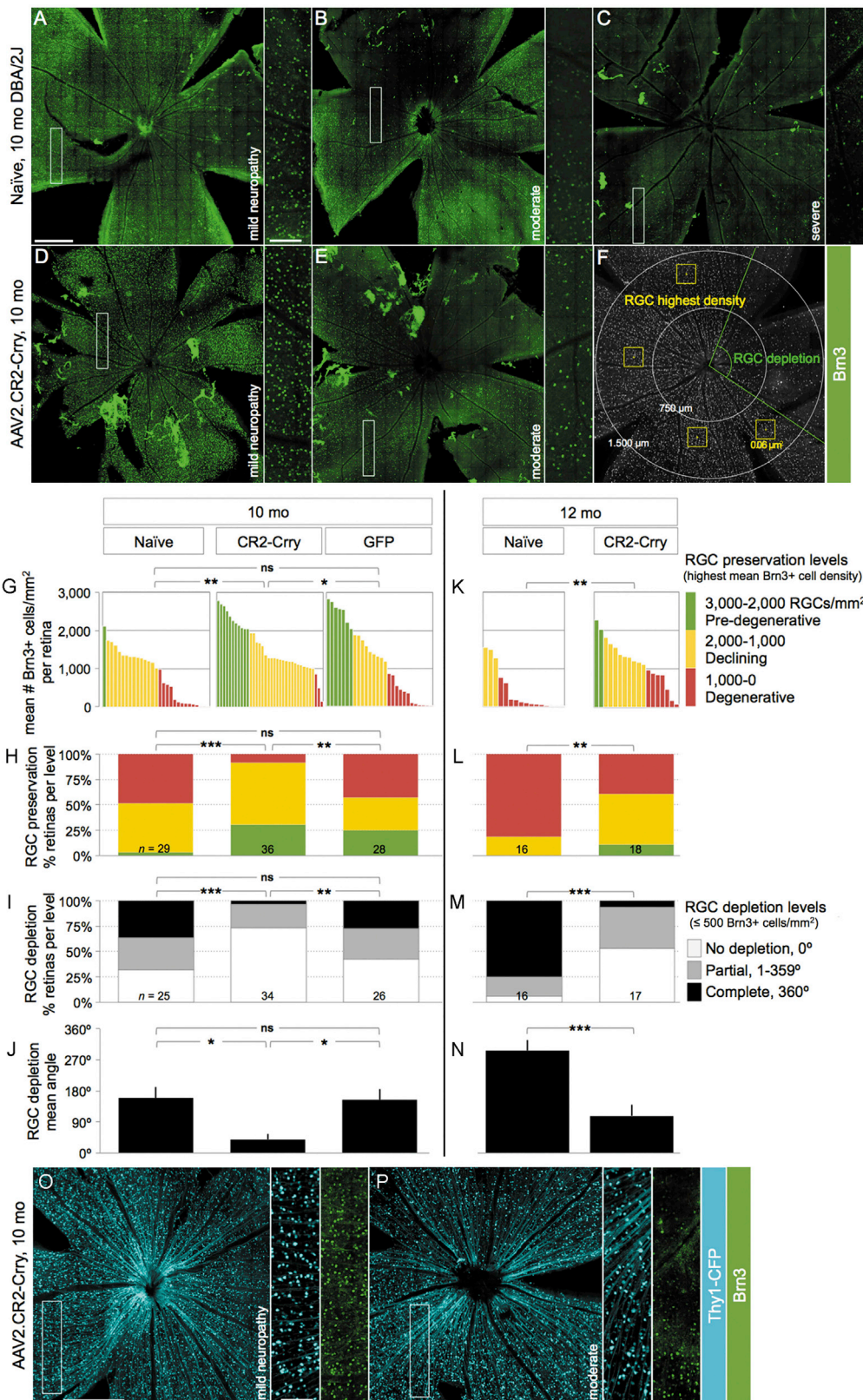
(legend on next page)

Table 3. Highest Mean Brn3+ Cell Density

	Normality (Shapiro-Wilk)	Kruskal-Wallis		Dunn's Multiple Comparisons Test	Kolmogorov-Smirnov	Mann-Whitney U
10-month-old naive	p = 0.006[a]		versus GFP	p = 0.2740	p = 0.103[b]	p = 0.1173[b]
			versus Crry	p = 0.0044[a]	p = 0.01[a,b]	p = 0.0009[a,b]
10-month-old CR2-Crry	p = 0.093	p = 0.0063[a]	versus GFP	p = 0.5066	p = 0.025[a,b]	p = 0.2036[b]
10-month-old GFP	p = 0.033[a]		–	–	–	–
12-month-old naive	p = 0.000[a]		versus Crry	p = 0.0042[a]	p = 0.0017[a,b]	p = 0.0005[a,b]
12-month-old CR2-Crry	p = 0.953	–	–	–	–	–

Statistical comparisons for mean number of Brn3+ cells/sq.mm per retina (Figures 2G and 2K).
[a]Significant differences.
[b]The values reported in the Results.

Table 7). AAV2.CR2-Crry-treated retinas showed significantly denser fascicles relative to naive DBA/2J retinas (3.3 ± 0.2 versus 2.6 ± 0.2 mean axons/fascicle for n = 20 and 26, respectively; p = 0.013 by an unpaired Student's t test) (Figure 3D, black line bar graphs; Table 7). Retinas injected with AAV2.GFP (n = 21) had a mean density (2.5 ± 0.2 axons/fascicle) that was significantly reduced compared to AAV2.CR2-Crry (p < 0.01), but not significantly different than naive eyes (p = 0.695; Table 7). Notably, AAV2.CR2-Crry retinas showed the most uniform high densities (none with less than 2.5 axons/fascicle and more than half the retinas with more than 3 axons/fascicle). These data were confirmed by post hoc Tukey's multiple comparison tests (Table 7).

To assess progression, we compared AAV2.CR2-Crry-treated eyes to naive at 12 months of age (Figure 3D). We observed that CR2-Crry-treated eyes showed progressive defasciculation relative to 10 months, but they maintained a mean of 2.6 ± 0.2 axons/fascicle, representing 1.7-fold more preserved axons per fascicle than age-matched naive retinas (1.52 ± 0.1 axons/fascicle, n = 15; p = 0.0016 by Kolmogorov-Smirnov; Table 7). The significant increase in axon fasciculation resulting from AAV2.CR2-Crry, although subtle, further highlights its protective effect.

Degeneration of the ON Is Reduced by Complement Inhibition

Since AAV2.CR2-Crry promotes preservation of Brn3+ RGCs and intraretinal axon fasciculation, we sought to determine whether this treatment could alter the course of axon degeneration.[64,65,70,72,73] We performed histological analysis of ON sections, and individual nerves were classified as pre-degenerative if their proximal cross-sec-

tion was dominated by dense intact axons, as moderately degenerative when >50% axons were healthy and 5%–50% were dystrophic, and as severely degenerative when >50% of axons were lost or dystrophic (Figure 4A). We then determined the ratio of nerves with pre-degenerative, moderate, or severe degeneration (Figure 4B). In naive untreated 7-month-old mice, the majority of nerves (96%) was pre-degenerative and none was terminally degenerative (4% moderate and 0% severe; n = 25), consistent with previous reports.[64] At 10 months, only half of naive nerves remained healthy (52% pre-degenerative) and the rest showed degeneration (10% moderate and 38% severe; total n = 83), which represents a significant change relative to 7 months (p < 0.01 by chi-square; Table 8). In contrast, AAV2.CR2-Crry therapy from 7 to 10 months nearly eliminated nerve degeneration (90% pre-degenerative, 6% moderate, and 4% severe; n = 53), a distribution that was not significantly different from naive 7-month-old mice by chi-square (p = 0.502). Relative to 10-month-old naive nerves, AAV2.CR2-Crry treatment resulted in almost twice as many healthy nerves (90% versus 52% pre-degenerative in naive), and it reduced by 10-fold the ratio of nerves at late stages of degeneration (4% versus 38% severe in naive) (p < 0.001; Table 8). Age-matched AAV2.GFP eyes also showed altered incidence of nerve pathology compared to naive, with an increased proportion of moderate and reduced proportion of severe nerves (53% mild, 29% moderate, and 18% severe; n = 34; p < 0.05; Table 8). However, nerve damage in 10-month-old AAV2.GFP controls was significantly worse than that of 10-month-old CR2-Crry-treated nerves (p = 0.001; Table 8).

We next sought to assess progression of axon degeneration by assessing the change in ON pathology over time (Figure 4C). Naive

Figure 2. AAV2.CR2-Crry Reduces Brn3+ RGC Degeneration Onset and Progression

(A–F) Confocal images through the NFL and GCL of retinal whole mounts immunostained for Brn3, shown as maximum-intensity projections of 25–35 μm. Insets display RGC mosaics at high magnification. Retinas representative of 10-month-old naive (A–C) and AAV2.CR2-Crry-treated mice (D and E), with corresponding level of ON damage indicated as pre-degenerative, moderately degenerative, or severely degenerative. (F) Example of Brn3+ cell-sampling method. (G and K) Plot of the highest density of Brn3+ RGCs (mean number nuclei/mm^2) for individual retinas at 10 (G) and 12 months (K) of age. (H and L) Stacked bar chart representing percent retinas at each level of RGC preservation per condition: pre-degenerative (mean Brn3+ RGC density/mm^2 >2,000, green), declining (1,000–2,000, yellow), and degenerative (<1,000, red). (I and M) Stacked bar chart representing percent retinas at each level of RGC depletion per condition: not depleted (0 degrees with less than 500 Brn3+ cells/mm^2, white), partial (1–359 degrees, gray), and complete (360 degrees, black). (J and N) Bar graph of mean depleted retinal area (degrees) per condition. (O and P) Confocal images of Thy1$^{CFP/+}$ RGCs from representative retinas of 10-month-old DBA/2J mice. Insets show their Brn3 co-expression at high magnification. Scale bars, 500 μm (A–F, O, and P) and 100 μm (insets). See Tables 3, 4, 5, and 6 for statistical analysis.

Table 4. Brn3+ RGC Preservation

	Chi-Square Test for Association	Test for Association	Goodness of Fit
10-month-old naive	versus GFP	p = 0.057[a]	p = 0.000[b]
	versus Crry	p = 0.000[a,b]	p = 0.000[b]
10-month-old CR2-Crry	versus GFP	p = 0.004[a,b]	–
10-month-old GFP	–	–	–
12-month-old naive	versus Crry	p = 0.0035[a,b]	p = 0.000[b]
12-month-old CR2-Crry	–	–	–

Statistical comparison for percent retinas by level of Brn3+ RGC preservation (Figures 2H and 2L).
[a]The values reported in the Results.
[b]Significant differences.

Table 5. RGC Depletion Level

	Chi-Square Test for Association	Test for Association	Goodness of Fit
10-month-old naive	versus GFP	p = 0.522[a]	p = 0.286
	versus Crry	p = 0.000[a,b]	p = 0.000[b]
10-month-old CR2-Crry	versus GFP	p = 0.009[a,b]	–
10-month-old GFP	–	–	–
12-month-old naive	versus Crry	p = 0.000[a,b]	p = 0.000[b]
12-month-old CR2-Crry	–	–	–

Statistical comparison for percent retinas by level of Brn3+ cell depletion (Figures 2I and 2M).
[a]The values reported in the Results.
[b]Significant differences.

DBA/2J nerves showed progressively worsening pathology from 10 to 12 months, and by 12 months most of the nerves were severely degenerative (22% pre-degenerative, 6% moderate, and 72% severe; n = 18) relative to 10 months of age (p < 0.01 by chi-square; Table 8). Nerves from AAV2.CR2-Crry-treated eyes also underwent a decline from 10 to 12 months of age (p = 0.001), but CR2-Crry maintained significant neuroprotection at 12 months with most of the nerves healthy (62% pre-degenerative, 23% moderate, and 15% severe; n = 39; p < 0.01; Table 8) relative to age-matched naive eyes. At 15 months of age, AAV2.CR2-Crry-treated nerves (n = 10) showed continued neuroprotection, with 60% pre-degenerative and only 20% moderately and severely degenerative each. Notably, AAV2.CR2-Crry-treated eyes were not significantly more degenerative at 15 months of age than at 12 (p = 0.974) or 10 months (p = 0.058). In previous studies of large cohorts of naive DBA/2J, approximately 75% of the ONs in females were severely damaged from 13 to 15 months of age.[64] In contrast, nerves from AAV2.GFP-treated eyes showed progression of degeneration from 10 to 15 months (p < 0.05; Table 8). Analysis of a limited set of AAV2.GFP nerves at 12 months (n = 8) showed widespread damage (25% pre-degenerative and 25% and 50% moderately and severely degenerative, respectively), and by 15 months AAV2.GFP nerves (n = 8) were progressively worse with 25% pre-degenerative, 13% moderately degenerative, and 63% severely degenerative (Table 8). Overall, these findings indicate that AAV2.CR2-Crry treatment suppressed glaucomatous ON degeneration in 10-month-old DBA/2J and persistently delayed its progression at 12 and 15 months of age.

AAV2.CR2-Crry Treatment Preserves Both Retina and ON in Individual Eyes

Finally, to determine whether there is similar protection of retina and nerve by AAV2.CR2-Crry in individual eyes, we compared mean Brn3+ RGC density versus level of ON degeneration per eye (Figure 4D). Analysis of 10-month-old naive eyes showed correspondence of damage levels between nerve and retina, with a decline in RGC density lagging behind nerve degeneration, suggested by declining retinas with similar intermediate densities having pre-degenerative or moderately degenerative nerves. In stark contrast,

age-matched AAV2.CR2-Crry-treated eyes showed preponderant preservation of pre-degenerative retinas with high to medium densities of RGC somata and matching pre-degenerative nerves. Unexpectedly, AAV2.GFP-treated eyes showed nerve protection uncoupled from retina preservation, manifest by degenerative retinas with nerves at all three stages of degeneration. At 12 months, naive eyes showed the expected terminal degeneration of both nerve and retina, evidenced by the prevalence of nerves at severe stage with retinas depleted of RGCs. At the same age, AAV2.CR2-Crry maintained its protective effect, as suggested by the relative high RGC densities with moderately damaged nerves. This comparison underscores that AAV2.CR2-Crry ocular therapy effectively reduces the progression of RGC axonal and somal decline and degeneration, protecting both the retina and its ON.

DISCUSSION

Addressing the need for treatment strategies that slow glaucoma progression, this study showed that retinal gene therapy of DBA/2J retinas with AAV2.CR2-Crry led to long-term overexpression of the Crry inhibitor and limited deposition of the C3d complement activation product on the GCL, which strongly preserved the integrity of both ONs and retinas in most eyes, despite concurrent IOP elevation. These findings define C3 activation-dependent complement signaling as a pathological driver of glaucomatous neurodegeneration, and also they establish AAV2.CR2-Crry as an effective gene therapy to locally correct pathogenic complement overactivation and restrict the onset and progression of neurodegeneration.

Targeting the C3 Activation Step for Complement Regulation

Dysregulated or excessive complement activation underlies multiple degenerative, inflammatory, and autoimmune pathologies, including neurodegenerative diseases.[34,74] In the expanding field of complement therapeutics,[75,76] diverse approaches targeting C3 activation have been shown to be efficacious and are being extended to human disease,[74,76] with some already in clinical trials,[75] including compstatin, a cyclic peptide that inhibits binding of C3 to the convertase.[74] Human CR1 is analogous to rodent Crry, and it has been linked to CR2 to generate a targeted C3 convertase inhibitor (TT32)[77] or modified to localize to the cell

Table 6. RGC Depletion

	Normality (Shapiro-Wilk)	Kruskal-Wallis		Dunn's Multiple Comparisons Test	Kolmogorov-Smirnov	Mann-Whitney U
10-month-old naive	p = 0.000[a]		versus GFP	p > 0.9999	p = 0.9992[b]	p = 0.6788
			versus Crry	p = 0.0025[a]	p = 0.0114[a,b]	p = 0.0005[a]
10-month-old CR2-Crry	p = 0.000[a]	p = 0.0011[a]	versus GFP	p = 0.0126[a]	p = 0.0168[a,b]	p = 0.0028[a]
10-month-old GFP	p = 0.000[a]		–	–	–	–
12-month-old naive	p = 0.000[a]		versus Crry	p = 0.0008[a]	p = 0.0005[a,b]	p = 0.0002[a]
12-month-old CR2-Crry	p = 0.001[a]	–	–	–	–	–

Statistical comparisons for mean degrees of Brn3+ cell depletion (Figures 2J and 2N).
[a]Significant differences.
[b]The values reported in the Results.

membrane (APT070).[33] In humans, C3 convertases can also be controlled via decay accelerating factor (DAF) and membrane cofactor protein (MCP),[78] with a chimeric human CR2-DAF shown to be highly effective at C3 inhibition in mice *in vivo*.[79] Thus, our findings showing the CR2-Crry can protect RGCs from glaucomatous neurodegeneration may ultimately be translatable to human glaucoma.

### AAV-Mediated Gene Therapy for Targeted CR2-Crry Delivery to the Retina

In vivo application of systemic CR2-Crry protein has been shown to ameliorate nervous system pathology in a spectrum of animal models.[40–43,80,81] In these models involving trauma, neuroinflammation, and ischemia, a disrupted blood-brain barrier allows access of the large CR2-Crry to the nervous system.[34] In glaucoma, complement activation is dysregulated at early stages when the retina-blood barrier is intact, which would prevent administered CR2-Crry protein from reaching C3d deposits. Retinal gene therapy, based on intravitreal injection of AAV vectors, bypasses retina-blood or other cellular barriers, and it locally supplies intrinsic, long-term expression of their cargo.[82] We showed that delivery of CR2-Crry via intravitreal AAV2 provided RGCs and the inner retina with a sustained Crry overexpression that regulated pathogenic C3 overactivation. Intraretinal administration of AAV2.CR2-Crry did not increase mortality or occurrence of external infections compared to naive mice (in over 50 treated mice; data not shown), suggesting no major systemic or off-target alterations in complement signaling or concomitant general immunosuppression. However, it remains possible that there are extraocular effects since intravitreally delivered AAV2 has the potential to reach blood and lymphatic tissue, as demonstrated in other animal models,[83] and it is able to induce innate and adaptive immune responses.[84] Locally, resident microglia are able to limit viral spread, and they induce a potentially neuroprotective effect secondary to this antiviral response.[85] There may also be an immune and/or inflammatory component caused by mechanical injury at the time of intravitreal injection of the viral vector.[86] Future studies will evaluate innate immune responses in AAV2-treated retinas, as well as the neuroprotective effects of their

microglia, since this may mediate the modest improvement detected in eyes treated with control AAV2.GFP.

Recombinant AAV-based therapeutics is prevalent in experimental and pre-clinical ocular gene therapy, due to the unmatched versatility, efficacy, and permanence of these vectors to transfer genes to the retina.[87,88] Treatments targeted to RGCs apply intravitreal AAV2 systems optimized to selectively transduce the inner retina.[47] For translation into the clinic, AAV2 has been modified to bypass the neutralizing mechanisms particular to humans,[89] and it proved safe and persistent for treating adult patients with chronic retinal disease.[90] The present study did not use AAV2-based retinal gene therapy to replace a defective RGC gene with a transgene, but to provide the glaucomatous retina with a targeted complement regulator aimed at steadily rebalancing the activation of a pathway central to the innate immune response that parallels chronic neurodegeneration.

The Complex Role of Local Complement Activation in Glaucoma

Knockout studies in DBA/2J glaucoma have suggested complex roles for the complement pathway in disease progression. C1q deficiency is protective against neurodegeneration,[27,28,30] but C3 deficiency is detrimental, with more severe nerves at 10.5, but not 12, months of age.[26] This suggests a harmful role for C1q and a neuroprotective role for C3.[26–28] In contrast, our study, which inhibits C3 activation but does not eliminate C3, suggests that local C3 activation contributes to RGC degeneration. This would be consistent with C1q and the classical pathway leading to C3 activation and contributing to pathology in glaucoma. It is possible that there are compensatory changes following C3 knockout that do not occur with local inhibition of C3 activation. The therapeutic value of targeted complement approaches based on tissue-specific inhibition, rather than systemic delivery or gene knockout, are supported by multiple studies.[8,33,34] Notably, C3 deficiency was protective against retinal ischemia-reperfusion, delaying axonal and RGC degeneration,[91] which implies a complex and more general role for complement activation following RGC injury. Therefore, when and where C1q and C3 are acting in glaucoma are still undefined. Future studies could apply inhibitors selective for each individual
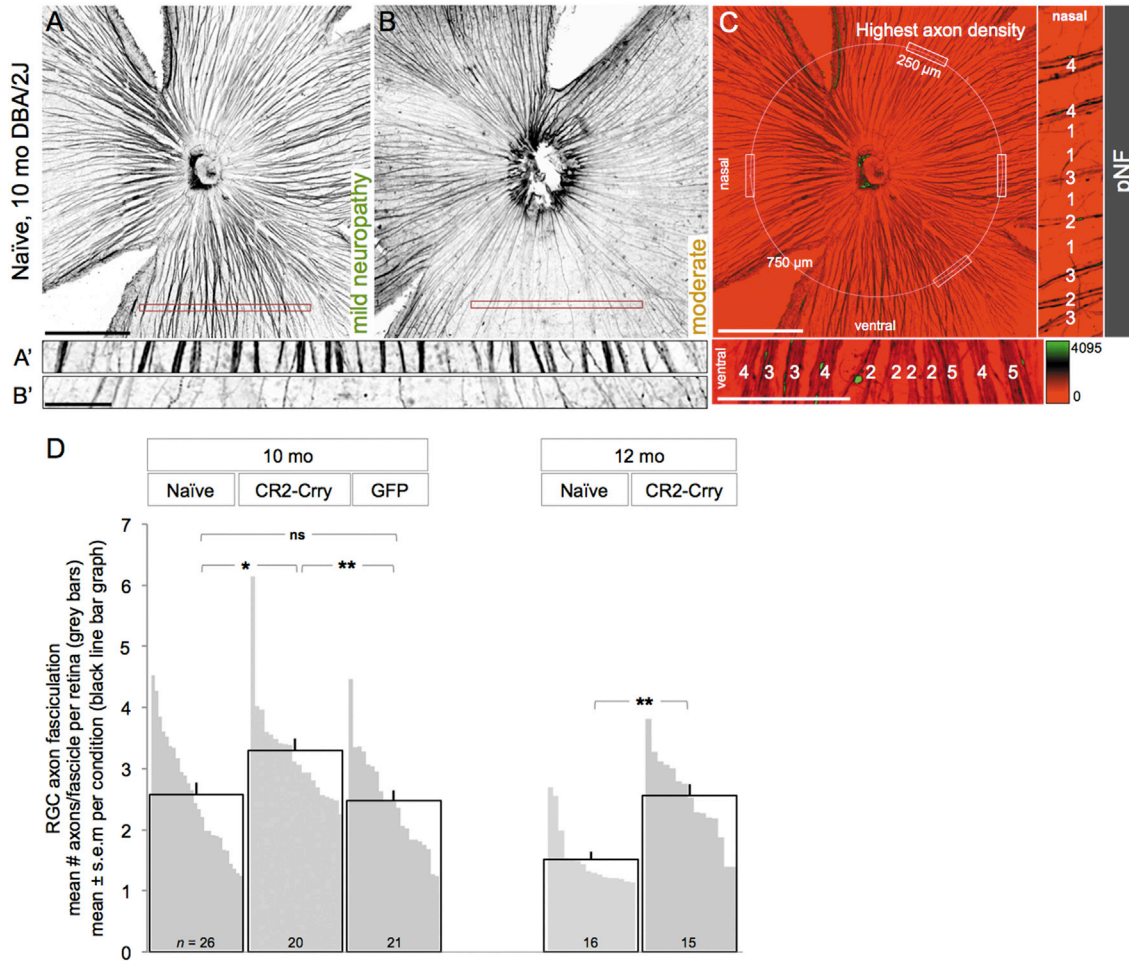
Figure 3. AAV2.CR2-Crry Protects Intraretinal Axons

(A–C) Confocal images of pNF-labeled RGC axons on retinal whole mounts, shown as 15-μm maximum-intensity projections through the NFL. Naive, 10-month-old retinas representative of a healthy NFL throughout all quadrants (A) and of an NFL with sectorial degeneration, detectable by fascicle thinning and loss (B). Insets show high-magnification views of retinal sectors with dense fascicles (A') and a degenerated sector with sparse, single axons, near depletion (B'). The corresponding level of optic neuropathy is indicated for each retina. (C) Sampling method for counting axon numbers per fascicle. Axons bundled together were counted within the healthiest radius of each quadrant, along a 250-μm line, 750 μm from the ONH. Analysis was done at high magnification in pseudocolored images (scaled by fluorescence intensity), as shown in the insets (numbers of axons per fascicle indicated for samples in the nasal and ventral quadrants). Scale bars, 500 μm (A–C) and 100 μm (insets). (D) Number of axons per fascicle expressed as mean per experimental group (black line bars) and as mean per individual retina (gray bars). For example, the retinas shown in (A) and (B) have, respectively, 3.4 and 2 axons/fascicle on average. See Table 7 for statistical analysis.

complement pathway to identify how each contributes to the course of glaucoma progression.

Complement Inhibition Restricts Onset and Progression of Axonal and Neuronal Degeneration

There is increasing evidence that degeneration of RGCs in glaucoma is compartmentalized, with distinct pathways driving axonal and somal decline programs and with distal axonopathy preceding cell body loss in the retina.[1,64,67,92] We observed that AAV2.CR2-Crry confers combined protection of both axons and somata, suggesting that complement activation mediates pathogenic events in both neuronal compartments. Onset of RGC degeneration in the DBA/2J is quite

variable, with axon damage histologically detectable from 8 to 12 months of age. By applying AAV2.CR2-Crry at 7 months of age, which is generally prior to overt structural decline, we were able to constrain complement activation preceding the onset of ON degeneration, and we assessed the effects on neurodegeneration onset and progression to terminal stage at 10–15 months of age. We observed highly significant preservation of ON integrity at 10, 12, and 15 months (3–8 months post-treatment), with a very low proportion of nerves showing severe damage. This indicates a conspicuous and continued reduction in the onset and terminal progression of pathology following complement inhibition (Figure 5). This protection resembles the phenotype of global C1q-knockout DBA/2J mice,[27,28]

Table 7. Intraretinal Axon Fasciculation

	Normality (Shapiro-Wilk)	One-Way ANOVA	Kruskal-Wallis		Tukey's Multiple Comparison Test	Unpaired t Test	Kolmogorov-Smirnov
10-month-old naive	p = 0.225			versus GFP	p = 0.9167	p = 0.6948[b]	p = 0.8306
				versus Crry	p = 0.0243[a]	p = 0.0129[a,b]	p = 0.0091[a]
10-month-old GFP	p = 0.396	p = 0.0083[a]	p = 0.0057[a]	versus Crry	p = 0.0127[a]	p = 0.0036[a,b]	p = 0.0076[a]
10-month-old CR2-Crry	p = 0.001[a]			–	–	–	–
12-month-old naive	p = 0.000[a]			versus Crry	p < 0.0001[a]	p < 0.0001[a]	p = 0.0016[a,b]
12-month-old CR2-Crry	p = 0.873	–	–	–	–	–	–

Statistical comparisons for mean number of axons per fascicle by condition and age (Figure 3D).
[a]Significant differences.
[b]The values reported in the Results.

in which severe nerve pathology was eliminated at 10.5 months and reduced to <25% at 12 months of age, suggesting delayed progression but ongoing neurodegeneration. The delay observed with AAV2.CR2-Crry is dramatic enough to offer significant potential therapeutic benefit. However, the fact that glaucoma pathology ultimately develops suggests that other pathways likely also contribute to the progression of neurodegeneration in glaucoma.

In glaucoma, the role of complement in RGC synapse remodeling and monocyte infiltration has largely been investigated in the DBA/2J model,[25,27,28] which is a well-characterized model of disease that exhibits many similarities to human disease, including age-dependent progression and sectorial loss.[93] However, it is possible that such immune and/or inflammatory responses are influenced by the loss-of-function mutation in *Gpnmb*, which is expressed in myeloid cell lineages, as recently reviewed.[94] Thus, testing AAV2.CR2-Crry gene therapy for the preservation of RGC and visual function in acute models of glaucoma will be important and may reveal roles for complement during active damage versus chronic progression. Future molecular studies should determine the cellular sources of complement proteins or inhibitors and define the responders, which will likely include resident microglia that express C3 receptors CR3 (CD11b/CD18, MAC-1) and infiltrating macrophages that carry recognition receptors to other complement components.[10] Recent studies suggest a dynamic capacity for microglia to sense and restrict neurodegeneration in a chronic disease such as Alzheimer's.[95] Consistent with this notion, our previous studies in DBA/2J glaucoma revealed the spatial proximity between microglia and all neuronal compartments of RGCs,[60] and they revealed the selective concentration of microglia in ONHs that were fated to develop severe neurodegeneration at advanced age.[63] How AAV2.CR2-Crry treatment modifies these innate immune responses will be the focus of future studies.

In summary, our study uncovers a damaging effect of C3 or downstream effectors in glaucoma, and it establishes AAV2.CR2-Crry as a precise and translatable strategy to locally balance retinal C3 activation and reduce neurodegeneration during the onset and progression of chronic glaucoma. From a clinical perspective, AAV vector delivery of targeted complement inhibitors offer an alternative to retinal gene therapies that simply replace damaged genes, by therapeutically regulating pathogenic complement pathways in chronic glaucoma, an approach that is applicable to other CNS neurodegenerative diseases.

## MATERIALS AND METHODS

Mice

Experimental work, handling, and care of mice were carried out in compliance with the ARVO Statement for the Use of Animals in Ophthalmic and Vision Research and under an animal protocol approved by the University of Utah Institutional Animal Care and Use Committee. DBA/2J and non-glaucoma control Gpnmb$^{+/+}$ DBA/2J mice were obtained from Jackson Laboratory (Bar Harbor, ME, USA) or bred in-house under sterile conditions, with 12/12 diurnal light cycles and food and water *ad libitum*. This study used females only, and each experimental group included similar numbers of mice born in Utah and Maine. Transgenic Thy1$^{CFP/+}$ DBA/2J mice, which express cyan fluorescent protein reporter under the Thy1 locus, were maintained by crossing to DBA/2J, using the original genotype to identify heterozygous offspring.[52]

AAV2 Vector Production

Recombinant, self-complementary AAV (scAAV2) with triple mutant capsids (Y444 + 500 + 730F) were generated by site-directed mutagenesis of surface tyrosine residues on the VP3 protein and prepared as previously described.[47,54] The titer of DNase-resistant scAAV2 vector genomes was measured by real-time PCR relative to a standard; purity was validated by silver-stained SDS-PAGE, sterility and absence of endotoxin were assayed, and aliquots were stored at −80°C and thawed no more than twice before use.

Intravitreal Injection

Mice were anesthetized by intraperitoneal injection of Avertin (1.3% 2,2,2-tribromoethanol and 0.8% tert-amyl alcohol, Sigma-Aldrich, St. Louis, MO, USA), and their eyes were anesthetized with topical tetracaine hydrochloride ophthalmic solution (Alcon, Forth Worth, TX, USA). A puncture through the wall of the eye was made at the posterior angle of the eye, below the limbus, with a 31G needle held by hand and observed under a dissecting microscope with fiber optic light. Immediately after, 2 μL AAV2 vector particles (10^{10} total
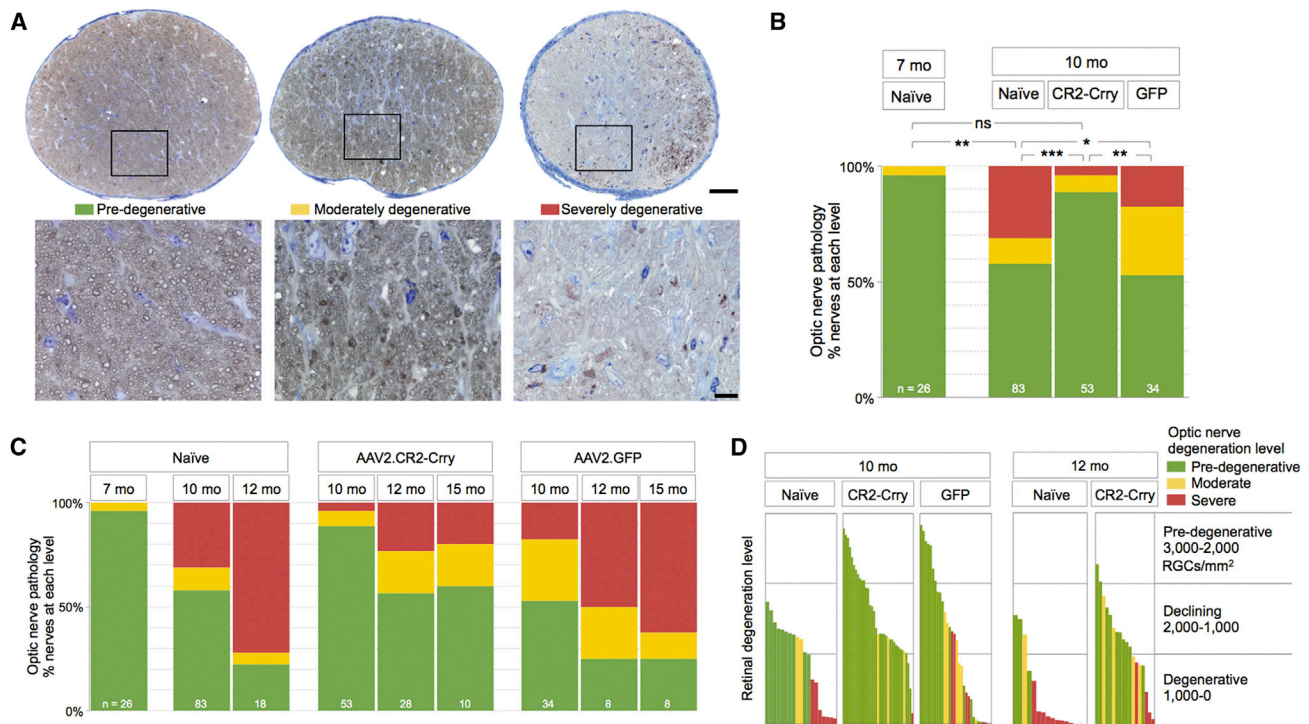
Figure 4. AAV2.CR2-Crry Suppresses Optic Nerve Neurodegeneration at 10 Months of Age and Reduces It at 12 and 15 Months

(A) Light microscopy images of retro-orbital ON cross-sections, each representative of mild, moderate, and severe damage levels in 10-month-old naive DBA/2J mice. Insets at higher magnification show that intact axons are recognizable by a clear axoplasm and intact myelin sheath, whereas dystrophic axons are detectable by a dark axoplasm and/or thick, delaminated myelin sheath. Scale bars, 50 μm (A) and 10 μm (insets). (B) Bar graph representing the distribution of ON damage by experimental group: pre- (green), moderately (yellow), and severely degenerative (red) by experimental group at 7 and 10 months of age (χ^2 test; sample size indicated). (C) Bar graph representing percent ONs at each level of pathology by condition and over time (sample size indicated). (D) Bar graph comparison of degeneration levels of retina versus ON for individual eyes. Each bar represents the mean Brn3+ RGC density for a single retina, and its color indicates the damage level of its ON. See Table 8 for statistical analysis.

vector genomes) was dispensed through this aperture using a blunt 34G needle attached to a 5-μL Nanofil Hamilton syringe run by an Ultra Micro Pump with Micro-4 controller (World Precision Instruments, Sarasota, FL, USA). After delivery of the vector at a rate of 1 μL/min, the needle was kept inside the eye for 60 s. Finally, the eyes were covered with erythromycin ophthalmic ointment (Bausch+Lomb, Rochester, NY, USA), and the animal was kept warm over a warm-water blanket until recovering full motility. Individual mice were injected with AAV2 expressing either the coding sequence of CR2-Crry or GFP from the chicken β-actin promoter (CBA).

IOP

IOP was determined as previously described.[96] Briefly, mice were sedated by inhalation of isoflurane via a Rodent Circuit Controller (VetEquip, Pleasanton, CA, USA), delivering 2% isoflurane in 2 L/min oxygen within a sealed box until lack of motility and through a nose cone afterward. Within 3 min of the start of anesthesia, 12 separate IOP measurements were performed using a Tonolab (Icare Tonovet, Finland), of which 10 were averaged (excluding the lowest and highest for each measure). Naive and treated mice had their IOP measured monthly from 7 to 10 months of age.

Tissue Collection and Fixation

Mouse eyes were collected as previously described.[68] Briefly, full anesthesia was induced by inhalation of 2% (vol) isoflurane in 2 L/min oxygen, and then mice were transcardially perfused with 5 mL PBS followed by 20 mL 4% paraformaldehyde (PFA; Electron Microscopy Sciences, Hatfield, PA, USA) in 0.1 M PBS, circulated with a peristaltic pump (Dynamax, Rainin, Oakland, CA, USA). Eyes and ONs were exposed *in situ* and post-fixed for 2 hr in PFA at 4°C, and then nerves were dissected and fixed overnight in 1.2% PFA and 0.8% glutaraldehyde in phosphate buffer (Electron Microscopy Sciences, Hatfield, PA, USA).

Whole-Retina qRT-PCR

Retinas were prepared and processed for RNA isolation not exceeding 10 min, as previously described.[68] Briefly, each individual retina was dissected fresh under RNase-free conditions, mechanically dissociated. As recently described,[96] RNA was isolated using the RNeasy micro kit (QIAGEN, Germantown, MD, USA), and its integrity was determined by Bioanalyzer (discarded <8) (Agilent, Salt Lake City, UT). We used Superscript III First Strand cDNA synthesis (Invitrogen, Carlsbad, CA, USA) and Nano-drop spectrophotometry (Thermo Fisher Scientific, Waltham, MA, USA). Real-time qPCR

Table 8. Statistical Comparisons for Proportion of Optic Nerve by Levels of Pathology (Figures 4B and 4C)

	Chi-Square Test for Association	Test for Association	Goodness of Fit
7-month-old naive	versus 10-month-old naive	p = 0.002[a,b]	
	versus 10-month-old Crry	p = 0.502[a]	
	versus 12-month-old Crry	p = 0.002[a,b]	–
	versus 15-month-old Crry	p = 0.016[a,b]	
10-month-old naive	versus 12-month-old naive	p = 0.005[a,b]	–
	versus 10-month-old GFP	p = 0.032[a,b]	p = 0.002[b]
	versus 10-month-old Crry	p = 0.000[a,b]	p = 0.000[b]
10-month-old CR2-Crry	versus 10-month-old GFP	p = 0.001[a,b]	
	versus 12-month-old Crry	p = 0.001[a,b]	–
	versus 15-month-old Crry	p = 0.058[a]	
10-month-old GFP	versus 12-month-old GFP	p = 0.139[a]	–
	versus 15-month-old GFP	p = 0.034[a,b]	
12-month-old naive	versus 12-month-old GFP	p = 0.324[a]	p = 0.049[b]
	versus 12-month-old Crry	p = 0.002[a,b]	p = 0.000[b]
12-month-old CR2-Crry	versus 10-month-old GFP	p = 0.214[a]	–
	versus 15-month-old Crry	p = 0.974[a]	
12-month-old GFP	versus 15-month-old GFP	p = 0.801[a]	–
15-month-old CR2-Crry	versus GFP	p = 0.179[a]	–

[a]The values reported in the Results.
[b]Significant differences.

reactions were prepared using SYBR Select Master mix (Thermo Fisher Scientific), and they were run on the 7900 HT Fast Real-Time PCR system with QuantStudio 12K Flex software (Applied Biosystems, Foster City, CA, USA). qPCR analysis was performed with the $\Delta\Delta C_t$ method to determine relative expression changes,[97] and gene expression was normalized to 3 housekeeping genes, including Gapdh, as well as Rik and Mrps6 that have consistent expression in the DBA/2J retina.[27] Primers were designed using Primer-BLAST software[98] as follows (forward primer first and reverse primer second): Gapdh: 5′-TGCACCACCAACTGCTTAGC-3′, 5′-GGCAT GGACTGTGGTCATGAG-3′; Cpsf7/5730453I16Rik: 5′-TGTCCCT CCTCCTCCTCCTG-3′, 5′-GGGGGAGGTACAGCCAGATG-3′; Mrps6: 5′-AATCCCTGATGGACCGAGGA-3′, 5′-TGTGCTGCTG GCTGTGACTC-3′; and Crry: 5′-CCAGCAGTGTGCATTGTCAG TCC-3′, 5′-CCCCTTCTGGAATCCACTCATCTC-3′.[99]

ON Histology, Imaging, and Analysis

Nerves were prepared as previously described.[73] Briefly, the postlaminar 1–1.5 mm of myelinated nerve was processed as 1-μm-thick plastic cross-sections, which were stained with toluidine blue to increase contrast for light microscopy and with paraphenylenediamine (PPD) to identify dystrophic myelin and axoplasm.[64] High-resolution multipoint (36 xy) images were generated using compound light microscopy and a 60× lens (BX51 and cellSens software, Olympus, Center Valley, PA, USA). Three authors, using images masked for

corresponding experimental group and retinal pathology, independently evaluated ON damage.

Retinal Histology and Immunofluorescence

Retinas were prepared as whole mounts the day after perfusion and immunostained as previously described the following day.[68,100,101] Briefly, whole-mount retinas were incubated with primary antibodies for 3 days at 4°C, then with secondary antibodies for 2 hr. Primary antibodies included the following: mouse anti-pNF (M07062 Dako, Carpinteria, CA, USA; diluted 1:100), mouse anti-non-phosphorylated neurofilament H, NF-H (801703 BioLegend, San Diego, CA, USA; diluted 1:500), goat anti-Brn3 (C-13, sc-6026 Santa Cruz Biotechnology, Santa Cruz CA, USA; diluted 1:50), and goat anti-C3d[59,60] (AF2655 R&D Systems, Minneapolis, MN, USA; diluted 1:1:500). Secondary antibodies included donkey anti-immunoglobulin G (IgG) Alexa Fluor 488, 555, and 647 nm (Invitrogen, La Jolla, CA, USA; diluted 1:400).

Confocal Imaging

Confocal images spanning entire retinal flat mounts were generated as previously described,[68,100] using a confocal imaging system equipped with a 20× lens and a resonant scanner (A1R confocal, Eclipse Ti inverted microscope and NIS-Elements C, Nikon). Multipoint images (625 xy positions) were acquired at high resolution (0.41 μm/pixel), then stitched and projected as maximal intensity of the inner 30–40 μm of retina (0.8-μm step). To allow image analysis and quantification, the parameters of image acquisition were maintained constant between retinal samples, and, for illustration, images had their brightness and contrast minimally edited.

Brn3-Expressing Cell Quantification

To estimate RGC preservation, we visually identified in each retinal quadrant the sector with densest Brn3+ nuclei at mid-periphery, where the number of Brn3+ nuclei was counted within a 250 × 250-μm box, masked to condition and age. The average of the four quadrants represents the mean density of preserved (highest) Brn3+ cells per retina, based on which individual retinas were considered as pre-degenerative ($\geq$2,000 cells/mm^2), declining (2,000–1,000 cells/mm^2), or degenerative ($\leq$1,000 cells/mm^2). To estimate RGC depletion, we measured the total extent of retinal sectors (in degrees of an angle with the apex at the ONH, with $\leq$500 Brn3+ nuclei/mm^2), classifying individual retinas as having no (0-degree), partial (1- to 359-degree), or complete (360-degree) depletion of Brn3+ RGCs.

Intraretinal Axon Fasciculation Quantification

The density of RGC axon fasciculation was analyzed in retinal whole mounts immunostained for pNF. Confocal images were projected at maximal intensity to span the entire NFL, and they were pseudocolored and zoomed 400× to facilitate the visualization of single axons. First, retinal sectors with preserved axon fasciculation were visually selected in each retinal quadrant, and a 250-μm-long line was traced perpendicular to the fascicles at an eccentricity of 750 μm (Figure 3C). Blind to experimental group, the number of pNF+ axons was counted
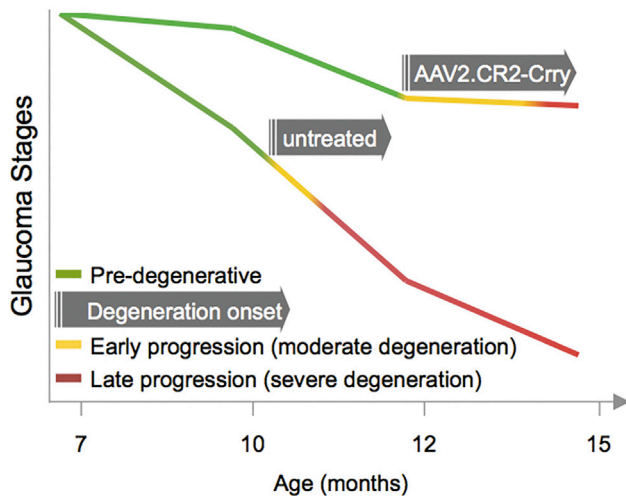
Figure 5. Glaucoma Progression after AAV2.CR2-Crry Retinal Gene Therapy

Diagram representing the delayed onset of ON and retinal degeneration and the slower progression in treated relative to naive DBA/2J mice.

along each of the four lines. Counts included axons bundled together in a fascicle, as well as defasciculated, single axons.

Statistical Analysis

All data were analyzed using statistical software (SPSS Statistics 23, IBM, Armonk, NY, USA) or GraphPad Prism (La Jolla, CA, USA). First, normality was determined by the Shapiro-Wilk test. Depending on the results of normality tests, either a one-way ANOVA or a Kruskal-Wallis test was used to determine differences across groups. Then a follow-up post hoc multiple comparison test was applied: Dunn's multiple comparisons for non-normal data or Tukey's for normal data. Normal datasets were further tested using Student's unpaired t test (with a Welch's correction if the variances between the two were significantly different). Non-normal datasets (Brn3+ cell density, mean degrees of Brn3+ RGC depletion, mean axon fascicles at 12 months, and IOP) were then further compared by two different non-parametric statistical tests, Kolmogorov-Smirnov and Mann-Whitney U. Differences in Brn3+ RGC preservation and depletion, as well as level of ON degeneration, were determined by a Pearson chi-square (χ^2) test for association; a χ^2 goodness of fit test also was run. We used a 95% confidence interval, and a p value of < 0.05 was set for rejecting the null hypothesis.

SUPPLEMENTAL INFORMATION

Supplemental Information includes two figures and can be found with this article online at https://doi.org/10.1016/j.ymthe.2018.08.017.

AUTHOR CONTRIBUTIONS

Conceptualization and Methodology, A.B. and M.L.V.; Investigation, A.B., S.R.A., K.T.B., C.O.R., M.R.S., V.A.C., and S.L.B.; Visualization and Writing – Original Draft, A.B.; Writing – Review & Editing, A.B.,

CONFLICTS OF INTEREST

W.W.H. and the University of Florida have a financial interest in the use of AAV therapies, and they own equity in a company (AGTC, Alachua, FL) that might, in the future, commercialize some aspects of this work. S.T. is an inventor on a licensed patent that covers CR2-targeted complement inhibitors, and S.T. has received royalties from Alexion (New Haven, CT).

REFERENCES

1. Calkins, D.J. (2012). Critical pathogenic events underlying progression of neurodegeneration in glaucoma. Prog. Retin. Eye Res. *31*, 702–719.

2. Jonas, J.B., Aung, T., Bourne, R.R., Bron, A.M., Ritch, R., and Panda-Jonas, S. (2017). Glaucoma. Lancet *390*, 2183–2193.

3. De Moraes, C.G., Liebmann, J.M., and Levin, L.A. (2017). Detection and measurement of clinically meaningful visual field progression in clinical trials for glaucoma. Prog. Retin. Eye Res. *56*, 107–147.

4. Levin, L.A., Crowe, M.E., and Quigley, H.A.; Lasker/IRRF Initiative on Astrocytes and Glaucomatous Neurodegeneration Participants (2017). Neuroprotection for glaucoma: Requirements for clinical translation. Exp. Eye Res. *157*, 34–37.

5. Soto, I., and Howell, G.R. (2014). The complex role of neuroinflammation in glaucoma. Cold Spring Harb. Perspect. Med. *4*, a017269.

6. Williams, P.A., Marsh-Armstrong, N., and Howell, G.R.; Lasker/IRRF Initiative on Astrocytes and Glaucomatous Neurodegeneration Participants (2017). Neuroinflammation in glaucoma: A new opportunity. Exp. Eye Res. *157*, 20–27.

7. Ricklin, D., Hajishengallis, G., Yang, K., and Lambris, J.D. (2010). Complement: a key system for immune surveillance and homeostasis. Nat. Immunol. *11*, 785–797.

8. Ricklin, D., Reis, E.S., Mastellos, D.C., Gros, P., and Lambris, J.D. (2016). Complement component C3 - The "Swiss Army Knife" of innate immunity and host defense. Immunol. Rev. *274*, 33–58.

9. Thielens, N.M., Tedesco, F., Bohlson, S.S., Gaboriaud, C., and Tenner, A.J. (2017). C1q: A fresh look upon an old molecule. Mol. Immunol. *89*, 73–83.

10. Stephan, A.H., Barres, B.A., and Stevens, B. (2012). The complement system: an unexpected role in synaptic pruning during development and disease. Annu. Rev. Neurosci. *35*, 369–389.

11. Zabel, M.K., and Kirsch, W.M. (2013). From development to dysfunction: microglia and the complement cascade in CNS homeostasis. Ageing Res. Rev. *12*, 749–756.

12. Orsini, F., De Blasio, D., Zangari, R., Zanier, E.R., and De Simoni, M.G. (2014). Versatility of the complement system in neuroinflammation, neurodegeneration and brain homeostasis. Front. Cell. Neurosci. *8*, 380.

13. Alawieh, A., Elvington, A., and Tomlinson, S. (2015). Complement in the Homeostatic and Ischemic Brain. Front. Immunol. *6*, 417.

14. Karlstetter, M., Scholz, R., Rutar, M., Wong, W.T., Provis, J.M., and Langmann, T. (2015). Retinal microglia: just bystander or target for therapy? Prog. Retin. Eye Res. *45*, 30–57.

15. Stasi, K., Nagel, D., Yang, X., Wang, R.F., Ren, L., Podos, S.M., Mittag, T., and Danias, J. (2006). Complement component 1Q (C1Q) upregulation in retina of murine, primate, and human glaucomatous eyes. Invest. Ophthalmol. Vis. Sci. *47*, 1024–1029.

16. Tezel, G., Yang, X., Luo, C., Kain, A.D., Powell, D.W., Kuehn, M.H., and Kaplan, H.J. (2010). Oxidative stress and the regulation of complement activation in human glaucoma. Invest. Ophthalmol. Vis. Sci. *51*, 5071–5082.

17. Mirzaei, M., Gupta, V.B., Chick, J.M., Greco, T.M., Wu, Y., Chitranshi, N., Wall, R.V., Hone, E., Deng, L., Dheer, Y., et al. (2017). Age-related neurodegenerative disease associated pathways identified in retinal and vitreous proteome from human glaucoma eyes. Sci. Rep. *7*, 12685.

18. Yang, X., Hondur, G., Li, M., Cai, J., Klein, J.B., Kuehn, M.H., and Tezel, G. (2015). Proteomics Analysis of Molecular Risk Factors in the Ocular Hypertensive Human Retina. Invest. Ophthalmol. Vis. Sci. *56*, 5816–5830.

19. Kuehn, M.H., Kim, C.Y., Ostojic, J., Bellin, M., Alward, W.L., Stone, E.M., Sakaguchi, D.S., Grozdanic, S.D., and Kwon, Y.H. (2006). Retinal synthesis and deposition of complement components induced by ocular hypertension. Exp. Eye Res. *83*, 620–628.

20. Miyahara, T., Kikuchi, T., Akimoto, M., Kurokawa, T., Shibuki, H., and Yoshimura, N. (2003). Gene microarray analysis of experimental glaucomatous retina from cynomologous monkey. Invest. Ophthalmol. Vis. Sci. *44*, 4347–4356.

21. Ahmed, F., Brown, K.M., Stephan, D.A., Morrison, J.C., Johnson, E.C., and Tomarev, S.I. (2004). Microarray analysis of changes in mRNA levels in the rat retina after experimental elevation of intraocular pressure. Invest. Ophthalmol. Vis. Sci. *45*, 1247–1258.

22. Johnson, E.C., Jia, L., Cepurna, W.O., Doser, T.A., and Morrison, J.C. (2007). Global changes in optic nerve head gene expression after exposure to elevated intraocular pressure in a rat glaucoma model. Invest. Ophthalmol. Vis. Sci. *48*, 3161–3177.

23. Panagis, L., Zhao, X., Ge, Y., Ren, L., Mittag, T.W., and Danias, J. (2010). Gene expression changes in areas of focal loss of retinal ganglion cells in the retina of DBA/2J mice. Invest. Ophthalmol. Vis. Sci. *51*, 2024–2034.

24. Steele, M.R., Inman, D.M., Calkins, D.J., Horner, P.J., and Vetter, M.L. (2006). Microarray analysis of retinal gene expression in the DBA/2J model of glaucoma. Invest. Ophthalmol. Vis. Sci. *47*, 977–985.

25. Stevens, B., Allen, N.J., Vazquez, L.E., Howell, G.R., Christopherson, K.S., Nouri, N., Micheva, K.D., Mehalow, A.K., Huberman, A.D., Stafford, B., et al. (2007). The classical complement cascade mediates CNS synapse elimination. Cell *131*, 1164–1178.

26. Harder, J.M., Braine, C.E., Williams, P.A., Zhu, X., MacNicoll, K.H., Sousa, G.L., Buchanan, R.A., Smith, R.S., Libby, R.T., Howell, G.R., and John, S.W.M. (2017). Early immune responses are independent of RGC dysfunction in glaucoma with complement component C3 being protective. Proc. Natl. Acad. Sci. USA *114*, E3839–E3848.

27. Howell, G.R., Macalinao, D.G., Sousa, G.L., Walden, M., Soto, I., Kneeland, S.C., Barbay, J.M., King, B.L., Marchant, J.K., Hibbs, M., et al. (2011). Molecular clustering identifies complement and endothelin induction as early events in a mouse model of glaucoma. J. Clin. Invest. *121*, 1429–1444.

28. Howell, G.R., MacNicoll, K.H., Braine, C.E., Soto, I., Macalinao, D.G., Sousa, G.L., and John, S.W. (2014). Combinatorial targeting of early pathways profoundly inhibits neurodegeneration in a mouse model of glaucoma. Neurobiol. Dis. *71*, 44–52.

29. Fernandes, K.A., Harder, J.M., Williams, P.A., Rausch, R.L., Kiernan, A.E., Nair, K.S., Anderson, M.G., John, S.W., Howell, G.R., and Libby, R.T. (2015). Using genetic mouse models to gain insight into glaucoma: Past results and future possibilities. Exp. Eye Res. *141*, 42–56.

30. Kumari, R., Astafurov, K., Genis, A., and Danias, J. (2015). Differential Effects of C1qa Ablation on Glaucomatous Damage in Two Sexes in DBA/2NNia Mice. PLoS ONE *10*, e0142199.

31. Howell, G.R., Soto, I., Ryan, M., Graham, L.C., Smith, R.S., and John, S.W. (2013). Deficiency of complement component 5 ameliorates glaucoma in DBA/2J mice. J. Neuroinflammation *10*, 76.

32. Mastellos, D.C., Reis, E.S., Ricklin, D., Smith, R.J., and Lambris, J.D. (2017). Complement C3-Targeted Therapy: Replacing Long-Held Assertions with Evidence-Based Discovery. Trends Immunol. *38*, 383–394.

33. Holers, V.M., Tomlinson, S., Kulik, L., Atkinson, C., Rohrer, B., Banda, N., and Thurman, J.M. (2016). New therapeutic and diagnostic opportunities for injured tissue-specific targeting of complement inhibitors and imaging modalities. Semin. Immunol. *28*, 260–267.

34. Alawieh, A., and Tomlinson, S. (2016). Injury site-specific targeting of complement inhibitors for treating stroke. Immunol. Rev. *274*, 270–280.

35. Molina, H. (2002). The murine complement regulator Crry: new insights into the immunobiology of complement regulation. Cell. Mol. Life Sci. *59*, 220–229.

36. Molina, H., Wong, W., Kinoshita, T., Brenner, C., Foley, S., and Holers, V.M. (1992). Distinct receptor and regulatory properties of recombinant mouse complement receptor 1 (CR1) and Crry, the two genetic homologues of human CR1. J. Exp. Med. *175*, 121–129.

37. Davoust, N., Nataf, S., Reiman, R., Holers, M.V., Campbell, I.L., and Barnum, S.R. (1999). Central nervous system-targeted expression of the complement inhibitor sCrry prevents experimental allergic encephalomyelitis. J. Immunol. *163*, 6551–6556.

38. Yang, P., Tyrrell, J., Han, I., and Jaffe, G.J. (2009). Expression and modulation of RPE cell membrane complement regulatory proteins. Invest. Ophthalmol. Vis. Sci. *50*, 3473–3481.

39. Atkinson, C., Song, H., Lu, B., Qiao, F., Burns, T.A., Holers, V.M., Tsokos, G.C., and Tomlinson, S. (2005). Targeted complement inhibition by C3d recognition ameliorates tissue injury without apparent increase in susceptibility to infection. J. Clin. Invest. *115*, 2444–2453.

40. Atkinson, C., Zhu, H., Qiao, F., Varela, J.C., Yu, J., Song, H., Kindy, M.S., and Tomlinson, S. (2006). Complement-dependent P-selectin expression and injury following ischemic stroke. J. Immunol. *177*, 7266–7274.

41. Alawieh, A., Elvington, A., Zhu, H., Yu, J., Kindy, M.S., Atkinson, C., and Tomlinson, S. (2015). Modulation of post-stroke degenerative and regenerative processes and subacute protection by site-targeted inhibition of the alternative pathway of complement. J. Neuroinflammation *12*, 247.

42. Hu, X., Tomlinson, S., and Barnum, S.R. (2012). Targeted inhibition of complement using complement receptor 2-conjugated inhibitors attenuates EAE. Neurosci. Lett. *531*, 35–39.

43. Qiao, F., Atkinson, C., Song, H., Pannu, R., Singh, I., and Tomlinson, S. (2006). Complement plays an important role in spinal cord injury and represents a therapeutic target for improving recovery following trauma. Am. J. Pathol. *169*, 1039–1047.

44. Cashman, S.M., Ramo, K., and Kumar-Singh, R. (2011). A non membrane-targeted human soluble CD59 attenuates choroidal neovascularization in a model of age related macular degeneration. PLoS ONE *6*, e19078.

45. Lenis, T.L., Sarfare, S., Jiang, Z., Lloyd, M.B., Bok, D., and Radu, R.A. (2017). Complement modulation in the retinal pigment epithelium rescues photoreceptor degeneration in a mouse model of Stargardt disease. Proc. Natl. Acad. Sci. USA *114*, 3987–3992.

46. Birke, M.T., Lipo, E., Adhi, M., Birke, K., and Kumar-Singh, R. (2014). AAV-mediated expression of human PRELP inhibits complement activation, choroidal neovascularization and deposition of membrane attack complex in mice. Gene Ther. *21*, 507–513.

47. Petrs-Silva, H., Dinculescu, A., Li, Q., Deng, W.T., Pang, J.J., Min, S.H., Chiodo, V., Neeley, A.W., Govindasamy, L., Bennett, A., et al. (2011). Novel properties of tyrosine-mutant AAV2 vectors in the mouse retina. Mol. Ther. *19*, 293–301.

48. Ju, W.K., Kim, K.Y., Duong-Polk, K.X., Lindsey, J.D., Ellisman, M.H., and Weinreb, R.N. (2010). Increased optic atrophy type 1 expression protects retinal ganglion cells in a mouse model of glaucoma. Mol. Vis. *16*, 1331–1342.

49. Bond, W.S., Hines-Beard, J., GoldenMerry, Y.L., Davis, M., Farooque, A., Sappington, R.M., Calkins, D.J., and Rex, T.S. (2016). Virus-mediated EpoR76E Therapy Slows Optic Nerve Axonopathy in Experimental Glaucoma. Mol. Ther. *24*, 230–239.

50. Berry, R.H., Qu, J., John, S.W., Howell, G.R., and Jakobs, T.C. (2015). Synapse Loss and Dendrite Remodeling in a Mouse Model of Glaucoma. PLoS ONE *10*, e0144341.

51. Cwerman-Thibault, H., Lechauve, C., Augustin, S., Roussel, D., Reboussin, É., Mohammad, A., Degardin-Chicaud, J., Simonutti, M., Liang, H., Brignole-Baudouin, F., et al. (2017). Neuroglobin Can Prevent or Reverse Glaucomatous Progression in DBA/2J Mice. Mol. Ther. Methods Clin. Dev. 5, 200–220.

52. Raymond, I.D., Pool, A.L., Vila, A., and Brecha, N.C. (2009). A Thy1-CFP DBA/2J mouse line with cyan fluorescent protein expression in retinal ganglion cells. Vis. Neurosci. 26, 453–465.

53. Williams, P.A., Harder, J.M., Foxworth, N.E., Cochran, K.E., Philip, V.M., Porciatti, V., Smithies, O., and John, S.W. (2017). Vitamin B₃ modulates mitochondrial vulnerability and prevents glaucoma in aged mice. Science 355, 756–760.

54. Petrs-Silva, H., Dinculescu, A., Li, Q., Min, S.H., Chiodo, V., Pang, J.J., Zhong, L., Zolotukhin, S., Srivastava, A., Lewin, A.S., and Hauswirth, W.W. (2009). High-efficiency transduction of the mouse retina by tyrosine-mutant AAV serotype vectors. Mol. Ther. 17, 463–471.

55. Thurman, J.M., Kulik, L., Orth, H., Wong, M., Renner, B., Sargsyan, S.A., Mitchell, L.M., Hourcade, D.E., Hannan, J.P., Kovacs, J.M., et al. (2013). Detection of complement activation using monoclonal antibodies against C3d. J. Clin. Invest. 123, 2218–2230.

56. Dräger, U.C., Edwards, D.L., and Barnstable, C.J. (1984). Antibodies against filamentous components in discrete cell types of the mouse retina. J. Neurosci. 4, 2025–2042.

57. Jakobs, T.C., Libby, R.T., Ben, Y., John, S.W., and Masland, R.H. (2005). Retinal ganglion cell degeneration is topological but not cell type specific in DBA/2J mice. J. Cell Biol. 171, 313–325.

58. Yun, S.P., Kam, T.I., Panicker, N., Kim, S., Oh, Y., Park, J.S., Kwon, S.H., Park, Y.J., Karuppagounder, S.S., Park, H., et al. (2018). Block of A1 astrocyte conversion by microglia is neuroprotective in models of Parkinson's disease. Nat. Med. 24, 931–938.

59. Alawieh, A., Langley, E.F., Weber, S., Adkins, D., and Tomlinson, S. (2018). Identifying the role of complement in triggering neuroinflammation after traumatic brain injury. J. Neurosci., 2197-17.

60. Natoli, R., Fernando, N., Jiao, H., Racic, T., Madigan, M., Barnett, N.L., Chu-Tan, J.A., Valter, K., Provis, J., and Rutar, M. (2017). Retinal Macrophages Synthesize C3 and Activate Complement in AMD and in Models of Focal Retinal Degeneration. Invest. Ophthalmol. Vis. Sci. 58, 2977–2990.

61. Michailidou, I., Naessens, D.M., Hametner, S., Guldenaar, W., Kooi, E.J., Geurts, J.J., Baas, F., Lassmann, H., and Ramaglia, V. (2017). Complement C3 on microglial clusters in multiple sclerosis occur in chronic but not acute disease: Implication for disease pathogenesis. Glia 65, 264–277.

62. Barnett, M.H., Parratt, J.D., Cho, E.S., and Prineas, J.W. (2009). Immunoglobulins and complement in postmortem multiple sclerosis tissue. Ann. Neurol. 65, 32–46.

63. Prineas, J.W., Kwon, E.E., Cho, E.S., Sharer, L.R., Barnett, M.H., Oleszak, E.L., Hoffman, B., and Morgan, B.P. (2001). Immunopathology of secondary-progressive multiple sclerosis. Ann. Neurol. 50, 646–657.

64. Libby, R.T., Anderson, M.G., Pang, I.H., Robinson, Z.H., Savinova, O.V., Cosma, I.M., Snow, A., Wilson, L.A., Smith, R.S., Clark, A.F., and John, S.W. (2005). Inherited glaucoma in DBA/2J mice: pertinent disease features for studying the neurodegeneration. Vis. Neurosci. 22, 637–648.

65. Anderson, M.G., Libby, R.T., Gould, D.B., Smith, R.S., and John, S.W. (2005). High-dose radiation with bone marrow transfer prevents neurodegeneration in an inherited glaucoma. Proc. Natl. Acad. Sci. USA 102, 4566–4571.

66. Soto, I., Oglesby, E., Buckingham, B.P., Son, J.L., Roberson, E.D., Steele, M.R., Inman, D.M., Vetter, M.L., Horner, P.J., and Marsh-Armstrong, N. (2008). Retinal ganglion cells downregulate gene expression and lose their axons within the optic nerve head in a mouse glaucoma model. J. Neurosci. 28, 548–561.

67. Buckingham, B.P., Inman, D.M., Lambert, W., Oglesby, E., Calkins, D.J., Steele, M.R., Vetter, M.L., Marsh-Armstrong, N., and Horner, P.J. (2008). Progressive ganglion cell degeneration precedes neuronal loss in a mouse model of glaucoma. J. Neurosci. 28, 2735–2744.

68. Bosco, A., Steele, M.R., and Vetter, M.L. (2011). Early microglia activation in a mouse model of chronic glaucoma. J. Comp. Neurol. 519, 599–620.

69. Domenici, L., Origlia, N., Falsini, B., Cerri, E., Barloscio, D., Fabiani, C., Sansò, M., and Giovannini, L. (2014). Rescue of retinal function by BDNF in a mouse model of glaucoma. PLoS ONE 9, e115579.

70. Howell, G.R., Libby, R.T., Jakobs, T.C., Smith, R.S., Phalan, F.C., Barter, J.W., Barbay, J.M., Marchant, J.K., Mahesh, N., Porciatti, V., et al. (2007). Axons of retinal ganglion cells are insulted in the optic nerve early in DBA/2J glaucoma. J. Cell Biol. 179, 1523–1537.

71. Wilson, G.N., Smith, M.A., Inman, D.M., Dengler-Crish, C.M., and Crish, S.D. (2016). Early Cytoskeletal Protein Modifications Precede Overt Structural Degeneration in the DBA/2J Mouse Model of Glaucoma. Front. Neurosci. 10, 494.

72. Bosco, A., Romero, C.O., Breen, K.T., Chagovetz, A.A., Steele, M.R., Ambati, B.K., and Vetter, M.L. (2015). Neurodegeneration severity can be predicted from early microglia alterations monitored in vivo in a mouse model of chronic glaucoma. Dis. Model. Mech. 8, 443–455.

73. Bosco, A., Breen, K.T., Anderson, S.R., Steele, M.R., Calkins, D.J., and Vetter, M.L. (2016). Glial coverage in the optic nerve expands in proportion to optic axon loss in chronic mouse glaucoma. Exp. Eye Res. 150, 34–43.

74. Morgan, B.P., and Harris, C.L. (2015). Complement, a target for therapy in inflammatory and degenerative diseases. Nat. Rev. Drug Discov. 14, 857–877.

75. Ricklin, D., and Lambris, J.D. (2016). New milestones ahead in complement-targeted therapy. Semin. Immunol. 28, 208–222.

76. Zipfel, P.F., and Skerka, C. (2009). Complement regulators and inhibitory proteins. Nat. Rev. Immunol. 9, 729–740.

77. Holers, M.V., Banda, N., Mehta, G., Fridkis-Hareli, M., Or, E., Storek, M., Altman, R., Johnson, K., and Katti, S. (2012). The human complement receptor type 2 (CR2)/CR1 fusion protein TT32, a targeted inhibitor of the classical and alternative pathway C3 convertases, prevents arthritis in active immunization and passive transfer models and acts by CR2-dependent targeting of CR1 regulatory activity. Immunobiology 217, 1210.

78. Jacobson, A.C., and Weis, J.H. (2008). Comparative functional evolution of human and mouse CR1 and CR2. J. Immunol. 181, 2953–2959.

79. Song, H., He, C., Knaak, C., Guthridge, J.M., Holers, V.M., and Tomlinson, S. (2003). Complement receptor 2-mediated targeting of complement inhibitors to sites of complement activation. J. Clin. Invest. 111, 1875–1885.

80. Elvington, A., Atkinson, C., Zhu, H., Yu, J., Takahashi, K., Stahl, G.L., Kindy, M.S., and Tomlinson, S. (2012). The alternative complement pathway propagates inflammation and injury in murine ischemic stroke. J. Immunol. 189, 4640–4647.

81. Qiu, S., Liu, N., Jia, L., Yang, G., Su, W., Li, J., Song, L., Yang, C., Wang, J., Zhang, C., et al. (2012). A new treatment for neurogenic inflammation caused by EV71 with CR2-targeted complement inhibitor. Virol. J. 9, 285.

82. Ochakovski, G.A., Bartz-Schmidt, K.U., and Fischer, M.D. (2017). Retinal Gene Therapy: Surgical Vector Delivery in the Translation to Clinical Trials. Front. Neurosci. 11, 174.

83. Seitz, I.P., Michalakis, S., Wilhelm, B., Reichel, F.F., Ochakovski, G.A., Zrenner, E., Ueffing, M., Biel, M., Wissinger, B., Bartz-Schmidt, K.U., et al.; RD-CURE Consortium (2017). Superior Retinal Gene Transfer and Biodistribution Profile of Subretinal Versus Intravitreal Delivery of AAV8 in Nonhuman Primates. Invest. Ophthalmol. Vis. Sci. 58, 5792–5801.

84. Reichel, F.F., Dauletbekov, D.L., Klein, R., Peters, T., Ochakovski, G.A., Seitz, I.P., Wilhelm, B., Ueffing, M., Biel, M., Wissinger, B., et al.; RD-CURE Consortium (2017). AAV8 Can Induce Innate and Adaptive Immune Response in the Primate Eye. Mol. Ther. 25, 2648–2660.

85. Drokhlyansky, E., Göz Aytürk, D., Soh, T.K., Chrenek, R., O'Loughlin, E., Madore, C., Butovsky, O., and Cepko, C.L. (2017). The brain parenchyma has a type I interferon response that can limit virus spread. Proc. Natl. Acad. Sci. USA 114, E95–E104.

86. Nakazawa, T., Nakazawa, C., Matsubara, A., Noda, K., Hisatomi, T., She, H., Michaud, N., Hafezi-Moghadam, A., Miller, J.W., and Benowitz, L.I. (2006). Tumor necrosis factor-alpha mediates oligodendrocyte death and delayed retinal ganglion cell loss in a mouse model of glaucoma. J. Neurosci. 26, 12633–12641.

87. Broadgate, S., Yu, J., Downes, S.M., and Halford, S. (2017). Unravelling the genetics of inherited retinal dystrophies: Past, present and future. Prog. Retin. Eye Res. *59*, 53–96.

88. Schön, C., Biel, M., and Michalakis, S. (2015). Retinal gene delivery by adeno-associated virus (AAV) vectors: Strategies and applications. Eur. J. Pharm. Biopharm. *95*, 343–352.

89. Bennett, J. (2017). Taking Stock of Retinal Gene Therapy: Looking Back and Moving Forward. Mol. Ther. *25*, 1076–1094.

90. Bennett, J., Ashtari, M., Wellman, J., Marshall, K.A., Cyckowski, L.L., Chung, D.C., McCague, S., Pierce, E.A., Chen, Y., Bennicelli, J.L., et al. (2012). AAV2 gene therapy readministration in three adults with congenital blindness. Sci. Transl. Med. *4*, 120ra15.

91. Kuehn, M.H., Kim, C.Y., Jiang, B., Dumitrescu, A.V., and Kwon, Y.H. (2008). Disruption of the complement cascade delays retinal ganglion cell death following retinal ischemia-reperfusion. Exp. Eye Res. *87*, 89–95.

92. Crish, S.D., Sappington, R.M., Inman, D.M., Horner, P.J., and Calkins, D.J. (2010). Distal axonopathy with structural persistence in glaucomatous neurodegeneration. Proc. Natl. Acad. Sci. USA *107*, 5196–5201.

93. McKinnon, S.J., Schlamp, C.L., and Nickells, R.W. (2009). Mouse models of retinal ganglion cell death and glaucoma. Exp. Eye Res. *88*, 816–824.

94. Lahola-Chomiak, A.A., and Walter, M.A. (2018). Molecular Genetics of Pigment Dispersion Syndrome and Pigmentary Glaucoma: New Insights into Mechanisms. J. Ophthalmol. *2018*, 5926906.

95. Keren-Shaul, H., Spinrad, A., Weiner, A., Matcovitch-Natan, O., Dvir-Szternfeld, R., Ulland, T.K., David, E., Baruch, K., Lara-Astaiso, D., Toth, B., et al. (2017). A Unique Microglia Type Associated with Restricting Development of Alzheimer's Disease. Cell *169*, 1276–1290.e17.

96. Breen, K.T., Anderson, S.R., Steele, M.R., Calkins, D.J., Bosco, A., and Vetter, M.L. (2016). Loss of Fractalkine Signaling Exacerbates Axon Transport Dysfunction in a Chronic Model of Glaucoma. Front. Neurosci. *10*, 526.

97. Schmittgen, T.D., and Livak, K.J. (2008). Analyzing real-time PCR data by the comparative C(T) method. Nat. Protoc. *3*, 1101–1108.

98. Ye, J., Coulouris, G., Zaretskaya, I., Cutcutache, I., Rozen, S., and Madden, T.L. (2012). Primer-BLAST: a tool to design target-specific primers for polymerase chain reaction. BMC Bioinformatics *13*, 134.

99. Radu, R.A., Hu, J., Yuan, Q., Welch, D.L., Makshanoff, J., Lloyd, M., McMullen, S., Travis, G.H., and Bok, D. (2011). Complement system dysregulation and inflammation in the retinal pigment epithelium of a mouse model for Stargardt macular degeneration. J. Biol. Chem. *286*, 18593–18601.

100. Bosco, A., Crish, S.D., Steele, M.R., Romero, C.O., Inman, D.M., Horner, P.J., Calkins, D.J., and Vetter, M.L. (2012). Early reduction of microglia activation by irradiation in a model of chronic glaucoma. PLoS ONE *7*, e43602.

101. Bosco, A., Inman, D.M., Steele, M.R., Wu, G., Soto, I., Marsh-Armstrong, N., Hubbard, W.C., Calkins, D.J., Horner, P.J., and Vetter, M.L. (2008). Reduced retina microglial activation and improved optic nerve integrity with minocycline treatment in the DBA/2J mouse model of glaucoma. Invest. Ophthalmol. Vis. Sci. *49*, 1437–1446.